

Surveying the Inner Solar System with an Infrared Space Telescope

Marc W. Buie

Southwest Research Institute, 1050 Walnut St., Suite 300, Boulder, CO 80302

B612 Foundation, 20 Sunnyside Ave., Suite 427, Mill Valley, CA 94941

`buie@boulder.swri.edu`

Harold J. Reitsema

B612 Foundation, 20 Sunnyside Ave., Suite 427, Mill Valley, CA 94941

`harold@b612foundation.org`

Roger P. Linfield

B612 Foundation, 20 Sunnyside Ave., Suite 427, Mill Valley, CA 94941

`rplinfield@comcast.net`

ABSTRACT

We present an analysis of surveying the inner Solar System for objects that may pose some threat to the Earth. Most of the analysis is based on understanding the capability provided by Sentinel, a concept for an infrared space-based telescope placed in a heliocentric orbit near the distance of Venus. From this analysis, we show 1) the size range being targeted can affect the survey design, 2) the orbit distribution of the target sample can affect the survey design, 3) minimum observational arc length during the survey is an important metric of survey performance, and 4) surveys must consider objects as small as $D = 15 - 30$ m to meet the goal of identifying objects that have the potential to cause damage on Earth in the next 100 years. Sentinel will be able to find 50% of all impactors larger than 40 meters in a 6.5 year survey. The Sentinel mission concept is shown to be as effective as any survey in finding objects bigger than $D = 140$ m but is more effective when applied to finding smaller objects on Earth-impacting orbits. Sentinel is also more effective at finding objects of interest for human exploration that benefit from lower propulsion requirements. To explore the interaction between space and ground search programs, we also study a case where Sentinel is combined with the Large Synoptic Survey Telescope and show the benefit of placing a space-based observatory in an orbit that reduces the overlap in search regions with a ground-based telescope. In this case, Sentinel+LSST can find more than 70% of the impactors larger than 40 meters assuming a 6.5 year lifetime for Sentinel and 10 years for LSST.

Subject headings:

1. Introduction

Near Earth Asteroids (NEAs) are a population of asteroids that spend at least part of the time in the inner solar system that are both potential

targets for future exploration missions and possible threats of Earth impact. Surveys for NEAs, notably NEAT (Pravdo *et al.* 1999), LINEAR (Stokes *et al.* 2000), Pan-STARRS (Jedicke *et al.* 2003, 2006) and the Catalina Sky Survey (Larson

2007), have found over 90% of NEAs larger than about 1 km in diameter and a total of over 13,000 of all sizes (Jedicke *et al.* 2015). Tedesco *et al.* (2000) and Cellino *et al.* (2004) presented the idea of space-based infrared survey instruments and the Earth-orbiting WISE telescope has now demonstrated NEA detection in infrared wavelengths from space, adding about 200 additional NEA discoveries (Mainzer *et al.* 2015b). Because of the power-law distribution of NEA sizes and following a recent re-examination of the population of small NEAs (Boslough *et al.* 2015), current estimates show that there are many times as many small NEAs that have not been found, perhaps as many as 4 million larger than 30 meters that could cause substantial damage upon impact. Chesley & Spahr (2004) and Vereš *et al.* (2009) considered the probability of impact of these small objects and demonstrated that impactors are likely to come from a limited range of orbital parameters, providing a sub-population of NEAs of most interest to planetary defense. This interest motivates the drive for better NEA searches for planetary defense. The National Research Council in 2010 recommended that “surveys should attempt to detect as many 30- to 50-meter objects as possible” (NRC Committee 2010). Such searches will also provide numerous targets that are within reach of available exploration mission launch and rendezvous capabilities.

Current surveys, while making clever and effective use of their facilities, are adding only about 2000 new discoveries per year. The rate of detection will rise by two orders of magnitude with the 2022 completion of the Large Synoptic Survey Telescope (LSST, Ivezić *et al.* 2007, 2014), which claims the potential to reach 82% completion on PHAs larger than 140 meters in 10 years. The LSST survey completion rate for smaller objects will be lower, 34% completion in 10 years down to Tunguska-like 40-meter objects. The Sentinel mission (Lu *et al.* 2013; Reitsema *et al.* 2014) is proposed to search for NEAs from a heliocentric orbit near Venus’ distance from the Sun (0.7 Astronomical Units, AU). As will be shown in this work, Sentinel surveys a unique volume of space and produces a complementary set of objects with a discovery rate even higher than that of LSST.

The goal of the present work was to understand how an infrared space-based observatory can

best be used to extend present-day surveys to a smaller size range for discovery of future impact threats. Working in the thermal infrared provides advantages for detecting NEAs since the target flux depends mostly on its heliocentric distance and much less on its albedo than does the visible flux. This property of an infrared survey provides a complementary aspect when run in parallel with optical surveys. Because of this weak dependence on albedo, infrared flux can more readily be used to deduce the size of the objects. Also, the phase angle dependence of brightness is less for thermal infrared observations than for visible reflectance. Additionally, the background source density is lower in the infrared, reducing difficulties due to confusing objects with background sources.

Presented here is an analysis of a series of mission options that include the baseline concept for the Sentinel Mission (Lu *et al.* 2013; Reitsema *et al.* 2014). There is no attempt here to demonstrate an optimal mission architecture: there are likely to be other designs that can work as well. The purpose of this work was to investigate Sentinel and see if it is sufficient to the task and also probe potentially beneficial variations in the mission design. Our statistical modeling method allows very fast execution and permits testing many different scenarios without requiring true exposure-by-exposure fidelity of a simulated detection dataset. Using this tool, the Sentinel design will be shown to be a very good approach for finding hazardous objects.

2. Baseline Mission Profile

The core of this work is an analysis of one particular mission design, called the baseline mission profile which represents the nominal properties of the Sentinel observatory. The top-level characteristics of the baseline mission are summarized in Table 1. The observatory is a wide-field infrared, fully steerable space-based telescope. The detectors employ Mercury-Cadmium-Telluride (HgCdTe) photo-sensitive material bonded to Capacitive Trans-Impedance Amplifier (CTIA) read-out circuits.

This choice of orbit was a consequence of optimizing the ability to detect NEAs. The orbit is also practical to achieve by taking advantage of a

TABLE 1
SENTINEL – BASELINE CAPABILITIES

Item	Value	Notes
Telescope Aperture	50 cm unobstructed	Passively cooled to 60K
Pixel Scale	2.15 arcsec/pix	Critically sampled on NEAs
Read noise	110 e-/pixel	per readout
Dark current	600 e-/sec	Active closed-cycle cooling to 30K
Field of View	2° by 5.5°	2x5 detector mosaic
Fill Factor	96%	small gaps between detectors
Wavelength	5 – 10.2 μ m	Unfiltered, set by detector
Exposure	180 sec	six 30-sec images
Field of Regard	Solar Elongation > 80°	set by sunshade
Observing Cycle	28 days	covers FOR four times
Cycle Cadence	0, 1h, 48h, 49h	two pairs
Semi-major axis	0.66 AU	Similar to Venus
Eccentricity	0.091	Not critical
Inclination	0.27°	Not critical

Venus gravity assist during the early phase of the mission. The orbital elements we use in modeling the baseline (V for Venus-like orbit) are nominal values used by the B612 Foundation’s industrial partner, Ball Aerospace, in their design work. The gravity assist is used to lower the aphelion distance and period of the orbit and the values shown in Table 1 reflect nominal values. The observatory is designed to function at any distance between Venus and Earth and the final orbit need not match the design values precisely. The angular elements used for the simulation are arbitrary. Also, we make no attempt to model the portion of the mission that will execute prior to the Venus flyby although routine survey operations are planned during the transit to Venus. The survey calculations assume the notional orbit for the entire duration of the mission.

The field of regard (FOR) covers slightly more than half the sky. The imaging system can cover this region 4 times in a 28-day observing cycle. The chosen observing location does come at a price. The distance from Sentinel to the Earth is too large for transmitting all data back for analysis, similar to the design of the Kepler Mission (Koch *et al.* 2010). Thus this design requires significant on-board processing to identify the moving objects in the data and then specify small re-

gions of interest (ROI) around the moving objects that will be transmitted to the ground. In reality, the on-board data processing is limited to the detection of transients in the image data that by its design will consist largely of moving objects. This on-board processing significantly reduces the volume of data that must be transmitted. These ROIs are the primary dataset from which final astrometry, linkages, and orbit estimations are generated in the ground system. More details about this aspect of the mission design can be found in Lu *et al.* (2013); Reitsema *et al.* (2014).

In our work, we describe the observations of an object as a 4-observation set collected in a 28-day observing cycle. This is an accurate description but can be mis-interpreted. Each observation is the result of combining six independent, back-to-back, images. These six “sub-images” are combined with a robust mean estimator that will eliminate any non-statistical outlier pixels. Only then is the combined image scanned for a detection above our signal-to-noise ratio threshold. Thus, these basic set of observations is really a 24-observation set where data have been aggregated down by a factor of six before transmission to the ground. While we discuss these observations as a pair of duples, there is considerably more data at work here. This method can deliver high-

confidence detections with very low false positive rates provided that the detectors are sufficiently stable. For the purposes of this study, we assume stability but this is clearly an issue that we must track very carefully during development of flight hardware.

3. Delivered Orbit Quality

An important outcome of the survey is not just a list of detected objects but linked observations of objects across multiple observing epochs and an estimate of their orbits. In the survey simulator, the number of observations of an object is tracked by counting the number of successful observing cycles and the time-span between the first and last cycle. A successful observing cycle is defined as one where the object is detected 4 times out of 4 opportunities within a cycle. If the object is detectable in an observing cycle but fails to be counted, the dominant reason for a failure is having the object fall on a chip gap in one or more observations. Generally, the variation in detectability from flux or target motion is small within a single observing cycle.

An essential component of a survey is clearly the ability to link observations from one detection to another. It was beyond the scope of this work to address the complete linkage problem. Instead, we make a few simplifying assumptions. The most important of these assumptions is that observations between different observing cycles can be linked. With the Sentinel cadence design, one cycle yields a 4-measurement track with a 2-day arc. Armed with the linkage assumption, we computed test cases that illustrate the orbit estimation quality as a function of the available data on an object.

For the following computations, a few sample object orbits were constructed. Given a set of observing times and an orbit, the spacecraft and object position are computed. To this is added measurement noise of 1.3 arc-sec per observation. This noise level is equal to 0.5 pixels and is estimated to be a conservative uncertainty that includes all sources of error from such components as centroiding, astrometric image solutions, and spacecraft location. These noise-injected values constitute a synthetic astrometric dataset that can be used to fit an orbit. Our tools are based on OpenOrb (Granvik *et al.* 2009). For short-arc fits we use

the OpenOrb statistical ranging Monte Carlo approach for the orbit and error estimations. Once the observation arc is long enough we can generate orbit fits and error estimation with the least-squares Gaussian estimation in OpenOrb. In this work we chose to use the Monte Carlo approach for data spanning 60 days or less and least-squares for longer arcs. We found that 60 days was the longest arc where statistical ranging was useful and used that even though the least-squares fitting also worked equally well over the high end of that range.

3.1. Short-arc data (≤ 1 hour arc)

The first case to consider is the accuracy of the orbit estimate and the ability to predict future positions given the first pair of observations. For the baseline Sentinel design, these two points will be separated by one hour. Table 2 contains a summary of the predictive power of this short-arc observation. The uncertainties are shown after converting to standard (tangent plane) coordinates, using the best-fit position as the tangent plane point – ξ is in the direction of right ascension (or ecliptic longitude) and η is in the direction of declination (or ecliptic latitude). Most of the Monte Carlo orbits generate positions in the same general area. However, some of the objects evolve significantly away from the cloud. These objects are those that happen to be very near the observatory at the time of observation and their future position can change very quickly. The implication from Table 2 is that an object needs to be seen again within a few days or it will be quickly lost. Note that the uncertainty in the position at the next planned observation in the survey cadence is roughly 4 arcmin (2 day predict). Based on our prior experience, the linkage to a second should be straightforward but simulations like these can be very useful to fine-tune the observing cadence if difficulties in making solid linkages arise.

3.2. Single Observing Cycle (2 day arc)

The second case is the orbit estimation and future position predictions based on a 4-observation set from a single observing cycle. In this case, the time spread in the observations is 2 days. Table 3 lists the predicted uncertainty versus the time since the last observation. The uncertainty region at short prediction times is a circular region

TABLE 2
SHORT-ARC (1-HOUR) DATA – FUTURE PREDICTIONS

Predict	σ_ξ (arcsec)	σ_η (arcsec)	Notes
1 sec	2.8	2.8	Region looks square, no outliers
1 min	2.8	2.8	Same region as for 1 sec predict
5 min	3.0	3.0	Region still looks square
10 min	3.3	3.3	Region still square, isolated outliers
15 min	3.5	3.6	Worst outliers at 15 arcsec
30 min	4.4	4.4	Region starting to round, worst at 30 arcsec
1 hr	6.8	6.2	Region even rounder, worst at 100 arcsec
2 hr	10	10	Region circular, worst at 800 arcsec
4 hr	18	18	worst at 34 arcmin
1 day	104	110	
2 day	229	251	Time of next observation
4 day	572	618	

NOTE.—This table shows one standard deviation of the sky-plane position (σ_ξ, σ_η) at different times (Predict) from the last observation. The notes describe the shape or other attributes of the uncertainty region of the object based on the orbit fit. Astrometric uncertainty assumed to be 1.3 arcsec per observation.

dominated by the size of the measurement errors. At longer prediction times the shape of the region is elliptical with a considerably smaller number of outlier objects than was the case for the 1-hour arc data. At the time of the next observing cycle, the positional uncertainty is substantial and linkages between the two observing cycles will need to use more than a positional coincidence between the object and the prediction to support the linkage. Additional information, such as orbit pole coincidence, rate of motion, direction of motion, as well as position will be required to make the linkage.

3.3. Multi-Cycle arc (≥ 28 days)

If an object is seen in two adjacent observing cycles, the orbit estimate gets much better. In OpenOrb, the orbit fitting can either be done with statistical ranging or traditional least-squares Gauss solutions. Table 4 shows how the positional uncertainty holds up over time for two observations in two adjacent observing cycles with a 28-day arc. At this point, the orbit estimate is becoming quite good and linkages to future observations is straightforward. Once three consecutive

cycles are linked the 10-year prediction is good to $\sigma_\xi = 37''$, $\sigma_\eta = 12''$. Thus the NEA position from 3 observing cycles is sufficient to permit targeted followup observations for physical characterization and high-precision orbit estimates.

3.4. Alternate Strategies

Table 5 summarizes the predicted positional uncertainty at the next epoch based on the data in hand for the baseline cadence. The column labeled N_{obs} provides the number of individual observations of the object. N_{cycles} indicates the number of observing cycles needed to get these observations. The column labeled “arc” gives the shortest possible arc-length of the observations. Note that spreading out a multi-cycle dataset for a longer arc with the same number of cycles will provide a better orbit estimate. The column labeled “predict” gives the length of time before the next possible observing opportunity. The final two columns give the uncertainty in the position for the time of the predict interval from the last observation. A special case is shown in the last line of a prediction for three-cycle dataset at 10 years from the obser-

TABLE 3
2-DAY ARC DATA – FUTURE PREDICTIONS

Predict	σ_ξ (arcsec)	σ_η (arcsec)	Notes
1 sec	2.1	2.0	circular uncertainty region
1 min	2.1	2.0	Same region as for 1 sec predict
1 hr	3.0	4.1	uncertainty region slightly non-circular
8 hr	14	18	uncertainty region definitely elongated
1 day	51	88	
8 day	1279	1897	
26 day	2.4°	3.2°	Time of next observation

NOTE.—This table shows the sky-plane uncertainty (σ_ξ, σ_η) at different times (Predict) from the last observation. The notes describe the shape or other attributes of the uncertainty region of the object based on the orbit fit. Astrometric uncertainty assumed to be 1.3 arcsec per observation.

TABLE 4
28-DAY (2-CYCLE) ARC DATA – FUTURE PREDICTIONS

Predict	σ_ξ (arcsec)	σ_η (arcsec)	Notes
1 hr	1.5	1.7	Error cloud dominated by measurement error
1 day	2.0	2.6	Worst error is 7 arcsec
2 day	2.5	3.7	Error cloud becoming elliptical
28 day	30	69	Elliptical error region
56 day	92	183	error region similar to a line-of-variation
1 yr	636	13	

NOTE.—This table shows the sky-plane uncertainty (σ_ξ, σ_η) at different times (Predict) from the last observation. The notes describe the shape or other attributes of the uncertainty region of the object based on the orbit fit. Astrometric uncertainty assumed to be 1.3 arcsec per observation.

TABLE 5
BASELINE CADENCE LINKAGE SUMMARY

N_{obs}	N_{cycles}	arc	predict	σ_{ξ} (arcsec)	σ_{η} (arcsec)
2	0.5	1 hr	2 day	229	251
4	1	2 day	26 day	8640	11520
8	2	28 day	28 day	30	69
12	3	56 day	28 day	2.0	3.7
12	3	56 day	10 year	37	12

NOTE.—This table shows the sky-plane uncertainty ($\sigma_{\xi}, \sigma_{\eta}$) at the time each linkage is made in extending the arc from discovery into being catalog. N_{obs} is the cumulative number of observations over N_{cycles} , where one cycle is 28-days that are used support each linkage. “Arc” gives the length of the constraining arc and “predict” gives the extrapolation time from last linked observation to the new data being linked. Astrometric uncertainty was assumed to be 1.3 arcsec per observation.

ventions.

The results in Table 5 can support an investigation into alternate cadences. The most important element of the survey process illuminated by this part of the analysis is the challenge of accurate linkages. The first linkage within the first observing cycle can be made easier by reducing the time between the first two pairs. If this time is reduced to 1 day, the positional uncertainty is reduced to $(\sigma_{\xi}, \sigma_{\eta}) = (127'', 155'')$ but this more than doubles the uncertainty at the next observing cycle, assuming the total number of observations remains constant. The only way to reduce the uncertainty at the time of the first cross-cycle linkage is to obtain more observations within an observing cycle. Making such a change affects the overall cadence but for this computation these changes are ignored. If an observing cycle were built from three pairs each separated by 30 minutes, the uncertainty at the next cycle is reduced by a factor of two. The cost of such a change is considerable and must be traded off against the need to make the linkage process easier. Discussions with the Minor Planet Center indicated that linkages even with the baseline cadence would be routinely possible and we did not pursue this issue any further. This assumption may well be worth further study but is beyond the scope of this work.

4. Detection

The survey simulator calculates the amount of collected thermal radiation from the NEA. If this is high enough above the background noise then the object can be detected. The signal collected is a combination of the thermal radiation and smearing from the PSF and any trailing losses. We ignore any contribution to reflected solar light in our passband.

4.1. Thermal Emission Model

The model for the thermal emission detected is a simple approximation to the problem. In general, the NEAs have a distribution of spin rates, rotation poles, and surface regolith properties but these details are ignored in favor of reasonable average values. The first step is to compute the isothermal surface temperature for the NEA based on radiative equilibrium. We used the thermal balance approximation for the temperature (eg. Spencer 1990) given by

$$T_{\text{NEA}} = \left(\frac{(1 - A)L_{\odot}}{r^2 4\epsilon\sigma} \right)^{\frac{1}{4}} \quad (1)$$

where A is the bond albedo, L_{\odot} is the solar constant ($1.374 \times 10^{-5} \text{ erg cm}^{-2} \text{ s}^{-1}$ from Willson *et al.* (1980)), r is the heliocentric distance [AU], ϵ is the emissivity of the surface, and

σ is the Stefan-Boltzmann constant [$\text{erg cm}^{-2} \text{s}^{-1} \text{K}^{-4}$]. The numeric factors in the denominator are based on the conservative choice of an isothermal model. The bond albedo is estimated from the geometric albedo using the phase integral from *Bowell et al.* (1989) and a phase coefficient of $G = 0.2$. The model approximates the variation in surface temperature from the sunlit and dark sides by the simple expression

$$T_{\text{BB}} = T_{\text{NEA}} + \Delta T \cos(\alpha) \quad (2)$$

where ΔT is a temperature correction factor and α is the solar phase angle. This expression gives the effective black-body temperature of the object at the given phase angle. The value of 30K for ΔT was chosen to match the actual brightness temperature for a rapidly rotating object with an intermediate thermal inertia and a mean sub-solar illumination direction.

The next step is to compute the monochromatic flux, F , incident on the observatory from the NEA by the Planck blackbody formula, diluted due to the NEA-observatory distance:

$$F = \frac{D^2}{4\Delta^2} \frac{2\pi hc^2}{\lambda^5 (e^{\frac{hc}{\lambda kT}} - 1)} \quad (3)$$

where D is the diameter of the NEA [km], Δ is the distance to the NEA from the observatory [km], h is Planck's constant [erg s], c is the speed of light [cm s^{-1}], λ is the wavelength of light [cm], k is Boltzmann's constant [erg deg^{-1}], T is the effective temperature of the NEA [K] taken from Eq. 2, and F is in units of [$\text{erg cm}^{-2} \text{s}^{-1}$]. To get the final detected signal, we integrated the black-body emission over the detector band pass, multiply by the area of the telescope, and multiply by 75% to include the reflectivity of the optics and the quantum efficiency of the detectors.

4.2. PSF and trailing losses

A Sentinel detection comes from seeing a change at a location in the sky. Such a change is assumed to be a consequence of an object moving across the field and being detected at different locations with each image. A detection kernel consisting of a 2x2 group of pixels is used that will contain flux from a moving object. A positive detection is thus one where the detection kernel

sees a change in the flux at a given position by more than 5σ above the background signal.

The image formed by a moving object is a trailed PSF. The trailing is caused by the apparent motion of the object during the exposure. Thus, the signal from the object may not fall in a single detection kernel if it is moving fast enough. The trailing fraction is the ratio of 2 (length of detection kernel) divided by the trail length in pixels. This ratio is capped at unity for very slow moving objects. The PSF chosen for the system further reduces the light in the kernel by 55%. Combining these two factors yields the fraction of the flux that is contained within the 2x2 pixel detection kernel. For the case of a 180 second exposure, any object moving slower than 0.57 degrees/day will incur minimal trailing losses. An object moving twice this rate will appear to be half as bright in a detection kernel for the same emitted flux.

4.3. Noise Sources

There are many sources of statistical fluctuations that limit the observations such as photon-counting noise from the object, detector readout noise, detector dark current, thermal background flux from the optics and telescope structure, and zodiacal light. Of these, the zodiacal light, or thermal emission from the dust in the plane of the solar system, is by far the dominant source of noise. Constant values for the adopted readout strategy are read-noise (110 e-/pixel/readout) and noise from dark-current (600 e-/sec). Transient noise sources caused by energetic particles hitting the detector are assumed to be eliminated by the readout pattern: each 180 second integration is the result of six 30-sec exposures that are combined in such a way as to eliminate the transients. The zodiacal emission is based on a model that integrates along the line-of-sight from the observatory in the plane of the ecliptic and over the wavelengths of the system passband. The three-dimensional dust cloud is described by an azimuthally symmetric form that decreases with increasing ecliptic latitude. This model ignores the fine structure such as dust bands, the Earth "ring", and the small tilt of the cloud with respect to the ecliptic (*Kelsall et al.* 1998). The area affected by the smaller scale structures will locally increase the background but this is ignored as a small perturbation on the full-sky survey. The tilt

of the cloud is also ignored for computational convenience. By ignoring this tilt, the angular elements of the NEAs and the spacecraft remain arbitrary. There is no net effect on the survey sensitivity when used as a statistical sampling tool.

Given the description of the dust distribution, we estimate the thermal radiation from the dust along any line of sight with a two-component model. The first component computes a detailed line-of-sight integral through the dust in the plane of the ecliptic. The second component is how the flux decreases with increasing ecliptic latitude of the look direction. This calculation was developed to quickly compute the background signal from any vantage point in the inner solar system near the ecliptic plane. The computed result tracks the background signal as a function of the heliocentric distance of the observatory, the angle from the anti-sun direction, and the angle from the ecliptic. Modeling a highly inclined observatory orbit would require adding a fourth dimension to the problem. This extra complexity was beyond the scope of this work but we have used an arbitrary factor of 2 reduction in the zodiacal dust brightness for the one inclined orbit case we considered. This approximation provides a useful bounding sensitivity test case but will not represent a rigorous result on the same footing as the orbit choices that are in the ecliptic.

The line-of-sight integral is estimated by computing the dust density and temperature along a line *in the ecliptic plane* and then determining the flux across the modeled bandpass. These integrations are quite slow and are not practical for embedding directly in the survey simulation tool. Instead, a grid of values on these two variables was computed from which interpolated values are drawn for the simulation.

We created a parameterized expression describing how the zodiacal emission falls off with increasing ecliptic latitude (β),

$$Z(\beta) = 1 - 0.919 \left\{ 1 - \frac{0.272}{|\sin \beta|} \left[1 - \exp \left(-\frac{|\beta|}{15.6^\circ} - \frac{1}{3} \frac{|\beta|^2}{(15.6^\circ)^2} \right) \right] \right\}. \quad (4)$$

Interpolated values from the table were merged with Eq. 4 to provide the background flux for any pointing of the observatory at the location of an

object to be detected. Example values from this calculation are plotted in Fig. 1. This figure shows the final signal in a detection kernel for two observatory heliocentric distances (0.7 and 1.0 AU) and at three different ecliptic latitudes ($\beta = 0^\circ, 30^\circ$ and 60°). The zodiacal background is higher when the observatory is closer to the sun and looking at lower solar elongations. For a similar look angle, the flux is roughly a factor of three higher at 0.7 AU than it is at 1.0 AU.

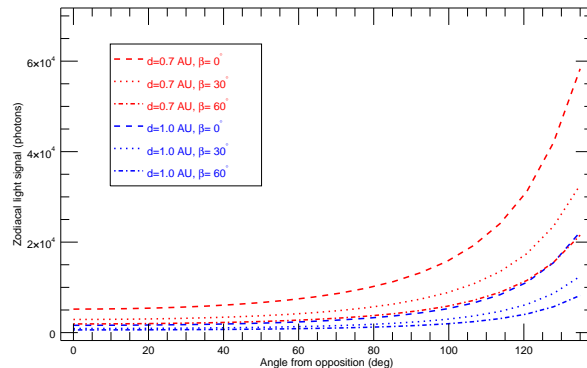


Fig. 1.— Signal from zodiacal dust in a detection kernel. The top three (red) curves show the zodiacal dust signal from a vantage point that is 0.7 AU from the sun. The bottom three (blue) curves show the signal that would be seen at the distance of 1.0 AU. Pairs of curves with similar line styles show the same ecliptic latitude look angle for the two distances.

The final SNR for an object is thus the object signal in the detection kernel divided by the combined noise from all the noise sources. To a very good approximation, it is sufficient to use just the object signal and the shot noise from zodiacal dust emission as the sole noise terms but we used all of these noise components in the model since the increase in computation time was negligible. We also investigated the effects of pixellation on the sampled image with a numerical experiment that places a source throughout a unit pixel and mapped this as a function of SNR. At high SNR, it is easy to see higher signal when the source is centered on the corner of a pixel. This geometry maximizes the flux in the 2x2 pixel detection kernel. At low SNR, this pixellation pattern disappears. The result is that regardless of SNR, a detection is equally likely at all fractional pixel locations.

One final effect was included in the simulations. Our flux and noise calculations give a theoretical estimate of the SNR for an observing cycle. Each opportunity for detection has its own noise, thus

an object at SNR=5 will be measured as having an SNR either lower or higher than this value. We conducted a numerical experiment to measure the odds of 4 successful detection given an expected SNR. Above SNR=9, the object is always detected and below SNR=3 the object is never detected with the survey threshold set to SNR=5. In between, the probability of 4 successful detections can be approximated to better than 1% with the following expression

$$P_{\text{SNR}} = 1 + \tanh((\text{SNR} - a)/b)/2 \quad (5)$$

where SNR is the expected signal-to-noise ratio for the source, and a and b are empirically derived factors. For SNR=5, we used $a = 5.99$ and $b = 0.74$. In our survey model, this expression was used for $3 < \text{SNR} < 9$ at each observing cycle to impose this detection probability on the synthetic observations. We compared these results to a simpler case where the probability is zero if SNR is less than the threshold and one if higher. The differences for the two cases is at most a few percentage points in differential completeness but is systematic in that the largest effect is at the detection limit. All of our results include the more complicated treatment since there is no effective computational penalty for its inclusion.

4.4. Fill Factor

The previous sections indicate if the object will meet or exceed the signal-to-noise ratio threshold for detection. The presence of small gaps between detectors can lead to a non-detection simply because the object happens to fall in a gap. For our baseline capabilities, we estimate that 4% of the FOV is taken up by gaps that are the boundaries between individual detectors in the mosaic. Early on in our work, we used a simple 96% probability of detection for each opportunity. Thus a successful set of four observations in an observing cycle had to all “miss the gap.” We were curious if there were patterns caused by the slightly non-random velocity vectors of objects lining up with chip gaps that could affect this simple probabilistic treatment. A full-fidelity simulation was added where the object is placed randomly on the FOV for the first of the four opportunities. The placement of the other three opportunities relative to the first was dictated by the orbital motion of

the spacecraft and object. All four of these positions were then checked against a model for the chip geometry and any position falling in a gap was removed from the detection list. The result of this more sophisticated treatment over the entire course of the survey gave the same answer as the simpler method. There was little change in execution time for the software so the more complicated method was used.

4.5. Successful Detections and Cataloging

Combining all of the components in the previous sections decides if an object is detected or not. For the four opportunities in each observing cycle, an object is counted as detected if $\text{SNR} \geq 5$ given its thermal emission flux relative to the sky background and detector noise sources and avoids the inter-chip gaps all four times. In this analysis we give no credit for a partial detection (eg., 3 out of 4 avoid gaps). In practice, these partial detections would be noted by the spacecraft and transmitted to the ground because they will still be valid transients. These data would ultimately provide some useful measurements despite being ignored for this analysis. In the end we require a successful detection in at least two observing cycles (total of eight detections) to consider an object cataloged.

5. NEA Model

To compute the results of a survey one must work with a model distribution of orbital elements of objects. There are two key components of this model: the distribution of orbital elements and the absolute number of objects as a function of size. These two components are described in the following two sub-sections.

5.1. Orbit Model

The most widely used model for NEA orbit distributions at present is Bottke *et al.* (2002). This model consists of orbital element bins organized by semi-major axis, eccentricity, and inclination and a probability of an object falling within that bin. Rather than render the distribution with discrete values of orbital elements, we chose to draw a random set of elements from the bin based on a uniform probability within the bin. At the time an orbit is drawn from the distribution, the three angular elements Ω , ω , and M are also chosen from a

uniform random number between 0 and 2π . All orbit calculations for this survey modeling are done with simple two-body motion.

5.2. Size Distribution

The survey model includes two methods for incorporating a size distribution for NEAs. One direct method is to associate a size with each orbit where the size is drawn from some approximation of the size-frequency distribution. This method becomes more computationally expensive when working to very small sizes. The second method is to do all of the survey calculations based on detection using a single fixed size. This type of value is called a differential completeness result and must be integrated over size to obtain the cumulative survey result typically used by other investigators. This result requires multiplying the computed differential completeness against the differential size distribution to return the integrated performance. This method is very handy in that the size of the object sample can be large enough per size bin to ensure good statistical sampling of performance.

In addition to the size-frequency distribution, one must also account for the range of surface albedo seen in the NEA population. Bottke *et al.* (2002) discuss a very simple bi-modal distribution where 9% of the objects have an albedo of 0.05 and the rest have an albedo of 0.103 for an absolute magnitude of $H_V \leq 18$. For fainter objects, 26% have the lower albedo and the rest have the higher albedo. This transition occurs at roughly $D = 1.5$ km. To support both types of survey calculations, a set of orbital elements must be generated equal to the total cumulative number of objects in the size distribution down to the smallest size to be considered. For this work we chose to fully model the distribution down to $D = 30$ m. At smaller sizes we are limited to using differential calculations.

Our current observational constraints on the size distribution have a photometric basis (apparent brightness) and are most strongly guided by reflected-light optical surveys. Thus, what we really have is a brightness distribution. Such distributions need to be converted to physical size before modeling can begin. It was beyond the scope of this work to properly convert from a brightness distribution to a true size distribution given the relatively poor state of knowledge of the actual

albedo distribution for sizes below a few hundred meters in diameter.

The size distribution of Boslough *et al.* (2015) was used to support this survey model and a sample of 3.5 million orbits was generated to support a cumulative calculation for $D > 30$ m. The value drawn from the distribution was the H_V magnitude according to the bounded probability function. Once a value for H_V was chosen, the albedo was selected from the two discrete values in accordance with the probability of those albedos given the size of the object.

5.3. Main Belt Asteroids

An NEA survey will also see main-belt asteroids (MBAs) during its operation. It is useful to estimate the expected number of MBA observations from a survey. Rather than use a synthetic distribution as with NEAs, we chose to use orbits and properties from known asteroids. Owing to their greater distance, there is no expectation of getting to the same small size regime as for NEAs. The known MBAs are complete enough to estimate the rate of re-detection for this purpose. These objects could also be used as calibrators for a survey for testing sensitivity and confirming any debiasing methods that would be applied to the NEA data. A secondary database table was built from all of the known asteroids using the astorb database developed by E. Bowell and now maintained by L. Wasserman at Lowell Observatory¹. This database includes assumptions or data regarding geometric albedo and phase function and this was used as is to compute physical sizes. The objects used were all those with multi-apparition orbits. The database for these tests was generated on Nov. 2013 at which time there were 536,261 objects.

5.4. Object and Orbit Sampling

The set of NEA orbits can be used either as a complete sample or they can be statistically sampled. To use the data as a complete sample, the entire list is run through the survey simulator with some size cutoff. This method permits directly sampling the survey properties on a cumulative size distribution with an embedded albedo distri-

¹<ftp://ftp.lowell.edu/pub/elgb/astorb.dat>

bution. Unfortunately, using a cumulative size distribution requires testing a very large number of orbits and the execution time can be prohibitively long.

An alternative is to use the orbits as a set from which to pull a statistically meaningful sample. In this way, a much smaller number of orbits can be used with substantial reduction in the run-time while ensuring good sampling at all sizes. The procedure used is to set a fixed size and albedo to a sub-sample of orbits and measure the survey properties. By running the simulator over a small number of discrete sizes and albedos, the differential completeness properties of the survey are measured. The quantity measured is the fraction observed as a function of time. The results presented here are based on 20,000 randomly chosen orbits from the full orbit sample. This sample size provides reasonably good statistics for the sizes considered here but some calculations at the smallest target sizes require an increase to counteract the low completeness values.

5.5. Sampling Other Object Types

The nominal set of NEA orbits from the Bottke distribution is a very diverse set of orbital elements. The only criterion applied for these objects is that their perihelion distance must be less than 1.3 AU — corresponding to a commonly accepted definition for a near-Earth asteroid. This set of objects is considered to be the baseline reference set due to the current Congressional challenge to NASA² and the scientific community³. The language at the time is most readily interpreted as referring to NEAs.

There are other subsets of objects worthy of consideration as well. These objects are contained within the set referred to as NEAs and their physical properties are generally considered to be the same. The most common subset is dubbed potentially hazardous asteroids (PHAs). These bodies are in orbits with minimum orbital

intersection distances (MOIDs) with respect to the Earth ≤ 0.05 AU. To support working with this subset, the MOID for each sampled object from the Bottke distribution was computed and saved to the database. Using the sampled set of orbits, the ratio of the number of PHAs to NEAs down to a given size is 0.202. Note that it is common to impose a lower size bound to objects labeled as PHAs. We do not include this cutoff in the analysis and only use the orbital properties to identify PHAs. To complete the usual set of sub-populations we also considered, Apollos ($q \leq 1.0167$, $a \geq 1$), Atens ($q < 1$, $Q \geq 0.983$), Earth-Crossing Asteroids (ECAs, Apollos+Atens), Amors ($a \geq 1$, $q > 1.0167$), and Atras ($a < 1$, $Q < 0.983$), where a is the semi-major axis of the orbit, q is the perihelion distance, and Q is the aphelion distance and all of these values are given in AU.

Another set of objects are those of interest as human exploration targets. Objects in these orbits are accessible to direct exploration via easier low-energy launches. Paul Chodas (personal communication) gave the orbit element range of $0.85 < a < 1.25$, $e < 0.17$, and $i < 6^\circ$ for orbits with $V_\infty \leq 2$ km/s that meet these requirements. We use this approximation of an orbital-element selection criterion for these objects due to the lack of actual knowledge of V_∞ within our simulator. This different samples of objects can be tested by modifying the database query to the appropriate set of orbital elements. The fraction of the NEA population that satisfy these constraints is rather small so a special sample was created to ensure the detection statistics would be accurate. This population is referred to in this work as the Asteroid Robotic Redirect Mission (ARRM) sample.

To better study objects that pose a more direct threat to Earth, we used the sample of virtual impactors (VIMP) that were published by Chesley & Spahr (2004) and Vereš *et al.* (2009). These orbits are drawn from the Bottke distribution but are determined to be orbits that result in an impact on the Earth with a uniform probability of impact over a 100 year time span. In keeping with this work, we have also adopted 100 years as a time-span of interest because it matches a human lifespan while also being a duration over which deterministic impact calculations can be made with sufficient supporting astromet-

²G. E. Brown, Jr., Near-Earth Object Survey Act. NASA Authorization Act of 2005 (Public Law No. 109-155), referred to hereafter as the GEB survey mandate.

³Near Earth Object Science Definition Team, 2003. Study to Determine the Feasibility of Extending the Search for Near-Earth Objects to Smaller Limiting Diameters. <http://neo.jpl.nasa.gov/neo/neoreport030825.pdf>, accessed 9/14/2015.

ric information. This also happens to match what the JPL Sentry system⁴ uses. This sample of impactor orbits contains 10,000 entries and require special care when used for very small sizes where the survey completeness is very low. For larger sizes this permits comparing mission profiles to evaluate their effectiveness in finding objects that are impactors within 100 years of the end of the survey.

All of these sub-populations must be scaled before computing the absolute numbers of detections and cumulative completeness. Table 6 provides the adopted scaling fractions for the sub-populations as represented in the Bottke *et al.* (2002) distribution compared to the full NEA population. These values are multiplied against the NEA size distribution curve from Boslough *et al.* (2015) to get the absolute size distribution curve for a sub-population. The second column lists the fraction of that sub-population compared to the total NEA population and is assumed to be independent of size. Using an impact probability for ECAs of 2.8×10^{-9} per year (W. Bottke, private communication) multiplied by the ECA fraction and by 100 gives an estimate of the total impacting flux on the Earth in a 100 year period. This last case is listed as Impactors but is also referred to as “VIMP.” The entries in the table are sorted by decreasing population. Note that when we model all of these populations, we consider the entire population and do not consider that some fraction of these are already known.

5.6. Field of Regard

The area in the sky that will be surveyed is called the field of regard (FOR). This region is defined in the baseline mission as running from 80° solar elongation to the anti-sun direction and over the full range of ecliptic latitude. The dwell time per field and the field of view (FOV) of the camera require 28 days to cover the entire FOR in the baseline mission. This cadence includes all slew and settling overhead plus operating margin and returns four observations of every location in the FOR per cycle.

In the simulator, the FOR can be varied by setting the range of ecliptic latitude and solar elongation to cover. Changing these ranges will al-

ter the time required to cover the FOR and thus change the time between successive observing cycles. The revised observing cycle time is scaled from the baseline 28 days by the ratio of the sky area coverage of the revised FOR to the sky area covered by the baseline FOR. We require that the arc-length for the observations be at least 28 days to tag an object as being cataloged.

6. Detection Efficiencies

In the simulator, each object is tested at each possible detection time for falling in a gap between detectors. The relative motion of the object between the individual observations is tracked but this set of opportunities is randomly placed on the FOV. If the object is bright enough to be detected, is in the FOR, and avoids the inter-chip gaps all four times it is counted as being detected in that observing cycle.

6.1. Differential Detection Efficiencies

The primary results from a simulation of the baseline Sentinel survey are summarized in Table 7. The absolute magnitudes (H_V) and the total number N_{NEA} come directly from Boslough *et al.* (2015). The tabulated diameter is the result of a simple conversion to size using a fixed geometric albedo of 14%. The values labeled with “N” give the current estimate of object greater than or equal to the tabulated diameter. The values labeled with “d” represent the completion percentage for the tabulated size – the differential completeness as described in section 5.2. The values labeled with “c” represent the cumulative completeness. The values labeled with “T” are estimates of the total number of objects to be cataloged by the survey. The values labeled with “NEA” are drawn directly from the (Bottke *et al.* 2002) distribution subject to the perihelion distance constraint ($a \leq 1.3$). The values labeled with “PHA” are drawn from the NEA distribution but also subject to the constraint of $\text{MOID} \leq 0.05$. The values labeled with “VIMP” represent the impactor population. The values with parentheses are provided in shortened form for exponential notation where the power of ten multiplier is given in parentheses. It’s worth considering that the NEAs have a much broader range of orbital properties compared to PHAs and

⁴<http://neo.jpl.nasa.gov/risk/>

TABLE 6
POPULATION NORMALIZATIONS

Type	N/ N_{NEA}	Orbit Constraint
NEA	1.	$q < 1.3$
ECA	0.683	Apollo+Aten
Apollo	0.623	$q \leq 1.0167, a \geq 1$
Amor	0.295	$a \geq 1, q > 1.0167$
PHA	0.202	$q < 1.3, \text{MOID} \leq 0.05$
Aten	0.0598	$q < 1, Q \geq 0.983$
Atira	0.0217	$a < 1, Q < 0.983$
ARRM	0.000348	$0.85 < a < 1.25, e < 0.17, i < 6^\circ$
Impactors	1.9×10^{-7}	Earth impactors

NOTE.—The fraction for impactors gives the number per century.

PHAs are much broader than VIMPs. NEAs include some objects that never get that close to the Earth (for example, $i = 80^\circ$, $e = 0.9$, and $q = 1.3$). Also, these relatively extreme orbits (particularly those with high eccentricity) have longer periods than the mission duration and some never get close enough to detect at all. A major result of this simulation is that our survey design reaches a significantly higher completion level for those objects that are a direct threat to the Earth than for the much broader and less threatening NEA population.

6.2. Cumulative Detection Efficiencies

An important outcome of the survey simulations is to quantify the absolute number of objects that will be detected. Converting from the differential values (d) to the cumulative values (c) requires integrating the product of d and the derivative of the Harris distribution. Table 7 shows these results. The integral is performed over H_V but a corresponding size (D) is shown for a fixed 14% geometric albedo. The cumulative number of NEAs down to the tabulated size is given in the column labeled N_{NEA} . These values directly replicate the Harris distribution. The next column gives the total number of PHAs and is based on a fixed fraction determined from the orbit distribution itself. In the Bottke *et al.* (2002) distribution, 20.2% of the NEAs are PHAs (see Table 6). The size depen-

dent cumulative completeness values and the total number of objects detected (T) are thus based on this calibration sequence. The completeness for the baseline survey and $D \geq 140\text{m}$ is 85% for NEAs, 87% for PHAs, and 95% for VIMPs. Clearly, the completeness of the survey diminishes with decreasing size. The 50% efficiency point lies between 60-100m for NEAs and PHAs but lies between 30-60m for VIMPs. Even though the differential completeness falls off dramatically at very small sizes, the total number of small objects that will be detected is substantial. Such a survey will be very well suited to a substantial refinement or confirmation of the size distribution over the range of sizes that represent significant threats to the Earth. Objects smaller than those tabulated are very unlikely to cause major damage upon impact.

The issue of albedo distribution presents a significant challenge when providing any cumulative results that indicate both size and absolute magnitude. It has become common to use 14% geometric albedo to convert between these two quantities but this is only an approximation. Showing results for a plot of cumulative detections really should have two separate curves, one for detections vs. size and one for detections vs. absolute magnitude. In the case of modeling optical surveys, this is an extremely important point. The detected flux for an object depends linearly on the albedo. As shown by Mainzer *et al.* (2011), the NEA albe-

TABLE 7
COMPLETENESS – BASELINE SURVEY

H_V	D (km)	N _{NEA}	N _{PHA}	N _{VIMP}	d_{NEA} %	d_{PHA} %	d_{VIMP} %	c_{NEA} %	c_{PHA} %	c_{VIMP} %	T _{NEA}	T _{PHA}	T _{VIMP}
26.9	0.015	34,600,000	7,000,000	6.6e+00	0.3	0.4	2.5	2.1	2.8	8	714,000	198,000	5.3e−1
26.3	0.020	15,800,000	3,200,000	3.0e+00	1.1	1.4	6.0	4.1	5.6	14	647,000	180,000	4.3e−1
25.4	0.030	4,790,000	970,000	9.2e−01	4.5	6.4	18	10	14	30	493,000	139,000	2.8e−1
23.9	0.060	513,000	104,000	9.8e−02	24	34	61	39	48	70	198,000	49,400	6.9e−2
22.8	0.100	142,000	28,700	2.7e−02	52	60	80	69	74	88	98,000	21,200	2.4e−2
22.1	0.140	75,800	15,300	1.4e−02	69	73	88	83	85	94	63,000	13,100	1.4e−2
21.3	0.200	46,100	9,300	8.8e−03	82	84	94	91	92	97	42,000	8,590	8.6e−3
19.9	0.380	19,600	4,000	3.8e−03	96	96	>99	98	98	>99	19,200	3,900	3.7e−3
17.8	1.000	4,440	898	8.5e−04	>99	>99	>99	>99	>99	>99	4,410	895	8.5e−4
16.9	1.514	2,230	450	4.3e−04	>99	>99	>99	>99	>99	>99	2,210	448	4.2e−4
15.9	2.399	951	192	1.8e−04	>99	>99	>99	>99	>99	>99	939	190	1.8e−4

NOTE.—Completeness values are given as a function of size and absolute brightness. The simulation and conversion from D to H_V was based on a fixed geometric albedo of 14%. The values labeled with “N” are absolute cumulative numbers for the different populations given by the subscript. The differential (single-size) completeness values are labeled with “ d ” and the cumulative completeness values are labeled with “ c ”. The columns labeled with “T” give the total cumulative number of objects detected.

dos are far from uniform with a range from 2-3% up to as high as 35%. For a given size, the observed brightness of an object is directly proportional to albedo making this a critical factor for proper modeling of optical surveys. The situation is not as extreme for thermal infrared detection surveys since the flux dependency on albedo is very weak in that it varies as the fourth root of albedo. Over this range of expected albedos for NEAs, the variation in detected IR flux is at most a 10% effect (Spencer 1989). For this reason, we chose to simplify our modeling by using a single albedo rather than a distribution to make it easier to understand the results versus both albedo and absolute magnitude, thus facilitating comparisons with past survey results. A more sophisticated treatment will change the absolute numbers by a small amount but the basic results we present will remain. In truth, the real distribution of NEA properties is more complex and the mapping of absolute magnitude to size is more complex. For the purposes of our survey design investigations, a simple mapping using a uniform 14% albedo was sufficient. It is clear to us, however, that there is a lot of merit in complementary surveys. Having a pair of surveys running, one in the optical and one in the infrared, is an excellent hedge against systematic detection biases when the goal is to find all the objects. These considerations are less important if the goal is merely to get enough objects to measure of the distribution after removing biases. In the case of Sentinel, the primary goal is to find objects and extracting a size distribution is of secondary importance.

6.3. Synodic Period Considerations

For a given simulator run, the synodic period was calculated for each object based on the observatory orbit. The sidereal periods are also computed. Any object whose sidereal or synodic period is longer than the mission duration could remain undetectable for the entire survey. This fraction of objects is really an upper limit to the number that can escape detection. For example, an object could be large enough to be detectable over the entire orbit and the synodic period would not matter. There are other intermediate cases where the object is detectable over enough of the synodic period that again it does not matter. Also, an object in a low-eccentricity orbit might always be

detectable whereas the same size object in a high-eccentricity orbit would be out of range for most of its orbit. Regardless of this complexity, the upper limit provides an indication of the fraction of the population that might never be seen. For the baseline mission, NEAs contain 2.7% with long synodic or sidereal periods, PHAs contain 1.6% that are too long, and VIMPs have only 1.2% in this category. Essentially all of the long-period VIMPs are long by virtue of their synodic periods with less than 0.01% having long sidereal periods. The complication of long synodic period objects appears to be a small component of the challenge of surveying the NEA population, at least for size ranges with low completion rates.

6.4. Modeling uncertainties

Our method of using differential completeness calculations was employed to minimize the numerical errors in the survey modeling. The counting errors in the model for a single size can be easily characterized and controlled and depend only on the number of objects in the sample. We standardized our calculations on 20,000 synthetic objects. This sample size results in completeness values good to $\leq 0.1\%$ down to $D = 30\text{m}$.

The uncertainties in the final cumulative completeness results is thus dominated by our limited knowledge of the actual properties of the NEA population. None of the distributions of size, albedo, thermal properties, pole position, and rotation periods are known perfectly well. We have used our own approximations for these values and different choices for these distributions will change the results by more than the sampling uncertainties in our model. For this reason, we do not delve more deeply into the modeling uncertainties as this really is a long-term research problem into the actual properties of NEAs and is beyond the scope of this work.

7. Alternate Survey Strategies

The survey simulator allows the exploration of survey designs other than the baseline mission concept. To speed up the exploration of parameter space, differential efficiencies at $D = 140\text{ m}$ and $D = 30\text{ m}$ are computed. From the cumulative results, the $D = 140\text{ m}$ efficiency should be around 85% to ensure a cumulative completeness of 90%.

This size is thus used to estimate if a given strategy meets the overall mission objectives as well as being an overall improvement or not. A second case of $D = 30\text{m}$, significant to Planetary Defense, is also computed to see if there are options that might excel at picking up smaller objects while not compromising the overall goal of getting a more complete census for $D \geq 140\text{ m}$.

The simulator permits altering many aspects of the survey: mission duration, telescope aperture, sky coverage (FOR), field-of-view, exposure time, detection threshold, and spacecraft orbit. Different asteroid orbit distribution models can also be used as they become available. The following subsections summarize the basic results of these survey variations compared to the baseline. The results from the analyses in this section are summarized in Table 8. The first case shown is the reference values for the baseline mission (V). The numbers shown are all given as percentages of differential completeness for the indicated diameter in meters for three classes of objects: NEAs, PHAs, and impactors. The columns labeled “syn” indicate the percentage of objects with synodic periods longer than the 6.5-year baseline mission duration.

7.1. Alternate Orbits

There are many orbital parameters that could be varied to investigate their potential for improved performance over the baseline Sentinel orbit. Interior orbits work well for providing a geometry very different from an Earth-based vantage point. As demonstrated earlier, the zodiacal background is higher with decreasing heliocentric distance for the observatory and is lower when working near the opposition region. These are two examples where the outcome of the change in orbit is not immediately obvious and the simulator can provide useful guiding information.

7.1.1. No Venus Gravity Assist

The baseline mission uses a Venus gravity assist to reduce the aphelion distance. This maneuver requires no fuel but it does impose timing constraints on the launch window. Without the gravity assist one can choose, using only the Earth-departure launch vehicle, a nearly arbitrary perihelion distance with aphelion at 1 AU, or, an ar-

bitrary aphelion distance with perihelion at 1 AU ($a=0.8\text{ AU}$, $e=0.25$). Orbits that extend beyond 1 AU were not investigated since that vantage point is severely handicapped for finding objects when they are interior to the Earth.

To investigate this option we chose an orbit with the same perihelion as the baseline orbit but an eccentricity that puts aphelion at 1 AU. Since the small end of the size range is limited by range to the target, this might have a chance to improve finding smaller objects that are in more Earth-like orbits. As shown in Table 8, the survey performance is worse for $D = 140\text{ m}$ regardless of the population tracked. The performance is also worse for $D = 30\text{ m}$ for NEAs and PHAs but is better for impactors. This option is denoted as mission option VE for the orbit carrying the observatory between the orbit of Venus and Earth. All other properties of Sentinel are kept the same.

Unfortunately, limitations in the current treatment of the zodiacal background prevent testing orbital options for a spacecraft that is significantly out of the ecliptic plane. A highly inclined orbit might be useful so that objects in the ecliptic are not seen against the strongest zodiacal emission in the plane. However, as seen in Fig. 1, the best this option can provide is roughly a factor of 2-3 reduction in background. As a proxy for this exploration, a case was investigated where the background flux is arbitrarily reduced in combination with a high-inclination orbit. The performance in this orbit was not markedly different from the performance of other cases studied and those model results are not discussed further.

7.1.2. Earth-similar Orbit

An even lower launch energy option is an orbit that puts it near the Earth. For the simulator it makes no difference if the observatory is in orbit around the Earth, at the L1 or L2 Lagrange points, or in an Earth-trailing or Earth-leading orbit. In reality, these options do place additional constraints on the accessible region of sky and how a survey might be carried out but these effects were ignored for this analysis.

Using an Earth-like orbit degrades the survey performance even more than the previous no-gravity-assist case (see Table 8). However, the degradation is less at the small end of the size

TABLE 8
COMPLETENESS TRADES

Case	NEA			PHA			Impactors			Notes
	d_{140}	d_{30}	syn	d_{140}	d_{30}	syn	d_{140}	d_{30}	syn	
V	69	4.5	2.6	73	6.4	1.7	88	18	1.2	Baseline mission
VE	61	3.1	3.6	65	6.0	3.3	81	21	5.5	No gravity assist
E	51	2.5	7.2	56	4.5	7.6	67	17	16	Earth-similar orbit
N	59	0.9	7.1	66	2.9	7.4	76	13	16	NEOcam FOR near Earth
V10	81	6.3	0.6	84	10	0.3	94	25	0.7	Case V for 10 years
VX	86	10	0.7	89	16	0.4	96	39	0.7	Enhanced Case V

NOTE.—The case shown is an abbreviation for the orbit or mission option studied (see text for details). The differential completeness (d) are shown for three sets of objects and the sub-script refers to the size, in meters, modeled. The column labeled “syn” indicates the percentage of the sample that has either a synodic period or orbit period greater than the 6.5 year the survey duration.

range. The penalty induced by long synodic period objects is noticeably worse for this option and is worst of all for the impactors. In this case, 15% of the VIMP sample has a synodic period longer than the 6.5 year survey.

Note that a space observatory located near the Earth will be observing a very similar subset of the population as is accessible to ground-based observatories at the same time – an asset if the survey goal is to get complementary thermo-physical observations. However, this orbit option is less desirable if the goal is to discover new objects as quickly as possible. This option is denoted as mission option E since the orbit is essentially the same as Earth. All other properties of Sentinel are kept the same.

7.1.3. Other Options

Also included in Table 8 is a case of an Earth-like orbit with a FOR similar to NEOCam as described in Mainzer *et al.* (2015a) and denoted as case N. The performance of case N is better than case E for NEAs and PHAs but worse for impactors. Case V10 is the same as the baseline mission but for a 10-year survey duration. Running the survey longer clearly improves the performance in all categories. Similar improvements would be seen for any orbit option. One final case, VX, is the baseline mission operating for 10 years with a 65-cm primary mirror. The FOV and pixel sampling relative to the diffraction limit is as-

sumed to be the same as the baseline mission. All other mission parameters remain the same. These last two cases are clearly higher-performance surveys but the changes to the mission would add significant costs to the mission.

7.2. Sky-plane Detection Maps

Understanding the result of a given choice of FOR is enhanced by looking at sky-plane maps where objects can be detected. To get this, the positions of all detectable objects are saved at each time step during a simulated survey. This information ignores the FOR within the survey run but includes source brightness, trailing losses, and background brightness. The pattern is collected in a coordinate system measured in ecliptic latitude and angle from the sun. This view will converge on a long-term average result. To get these views, the survey was run as long as needed to build up meaningful statistics. For clarity, the region within 25° of the Sun is suppressed. These results are much more informative when computed for a single size range at targeted sizes.

Figure 2 shows sky-plane detection maps for NEAs at a few strategic sizes for the baseline Sentinel mission. These images show relative likelihoods of detection for a single size of object as indicated with the most likely location being normalized to unity. The objects are largely concentrated within $\pm 30^\circ$ of the ecliptic. The contributions near the ecliptic poles never drop to zero but

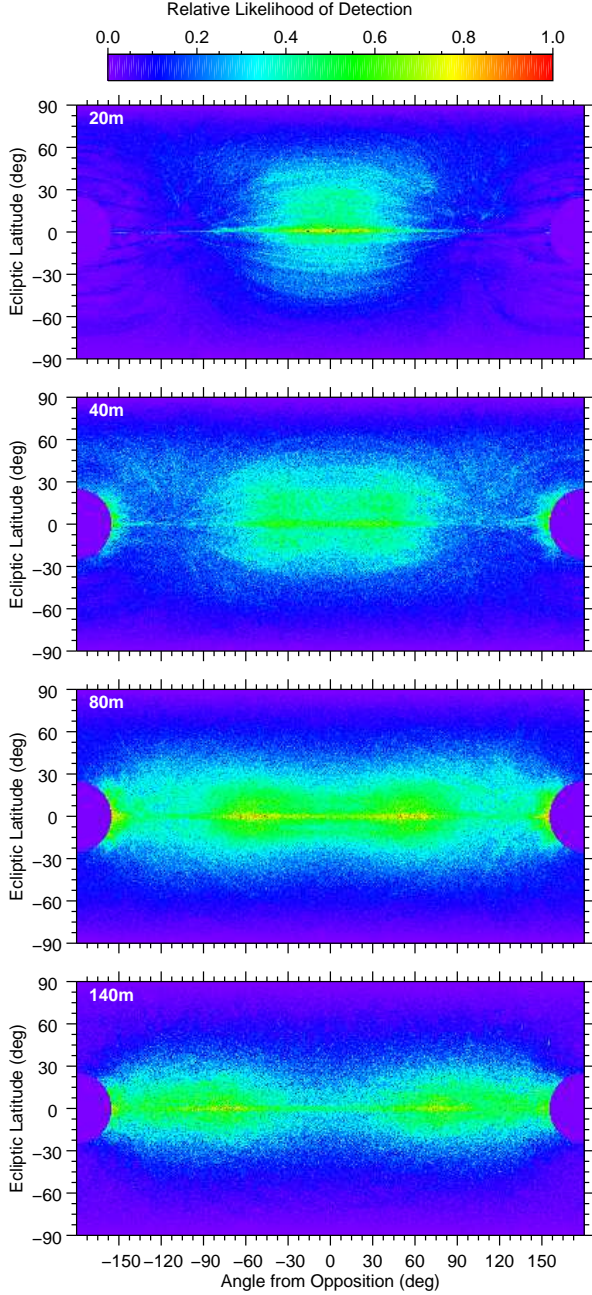


Fig. 2.— Detectability map for Near-Earth Asteroids with the nominal Sentinel design (V) for different target sizes. Each panel shows where in the sky a target of the given size can be detected. The top panel is for the smallest objects with $D = 20$ m and the bottom panel is for $D = 140$ m. Each map is normalized to 1 at the most likely location. Points with 25° of the Sun are set to zero. This sequence clearly shows a transition from favoring quadrature for detecting larger objects to opposition for detecting small objects.

is much less than along the ecliptic. Most interesting is the trend with object size. The $D=140$ m map at the bottom of the figure shows that the regions near quadrature are favored for object

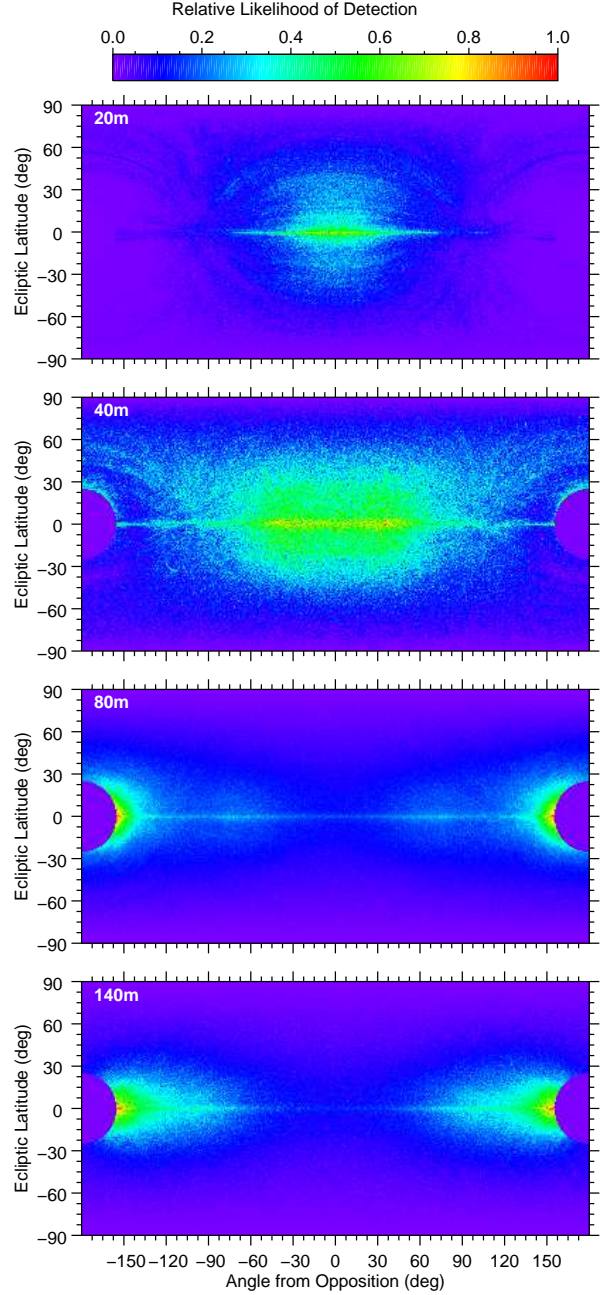


Fig. 3.— Detectability map for Near-Earth Asteroids with the mission option E for different target sizes. Each panel shows where in the sky a target of the given size can be detected. The top panel is for the smallest objects with $D = 20$ m and the bottom panel is for $D = 140$ m. Each map is normalized to 1 at the most likely location. Points with 25° of the Sun are set to zero. At this heliocentric distance, detections are more likely at lower solar elongation angles as the object size increases.

detection. As the object size decreases there is a marked change in the pattern to where the opposition region is strongly preferred once the size drops to $D = 20$ m. This trend has been reported

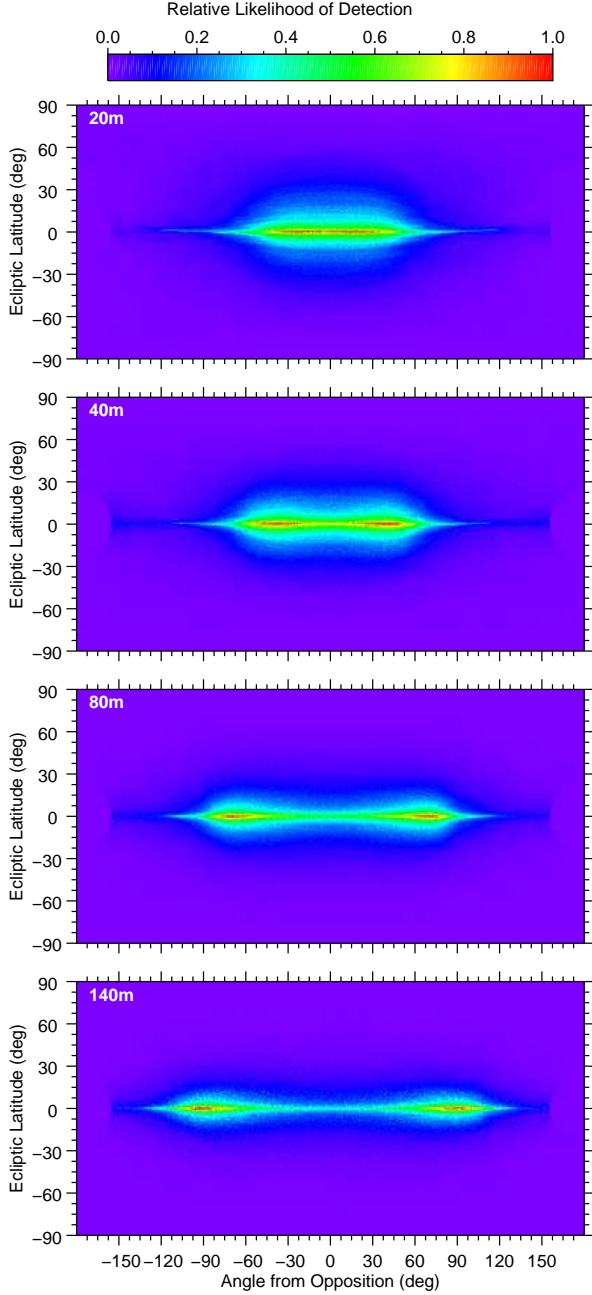


Fig. 4.— Detectability map for virtual impactors with the nominal Sentinel design (V) for different target sizes. Each panel shows where in the sky a target of the given size can be detected. The top panel is for the smallest objects with $D = 20$ m and the bottom panel is for $D = 140$ m. Each map is normalized to 1 at the most likely location. Points with 25° of the Sun are set to zero. This sequence clearly shows a transition from favoring quadrature for detecting larger objects to opposition for detecting small objects.

before with a more limited representation for the optical (Jedicke 1996; Chesley & Spahr 2004). The patterns we show will also hold for optical observations but with shifts relative to the

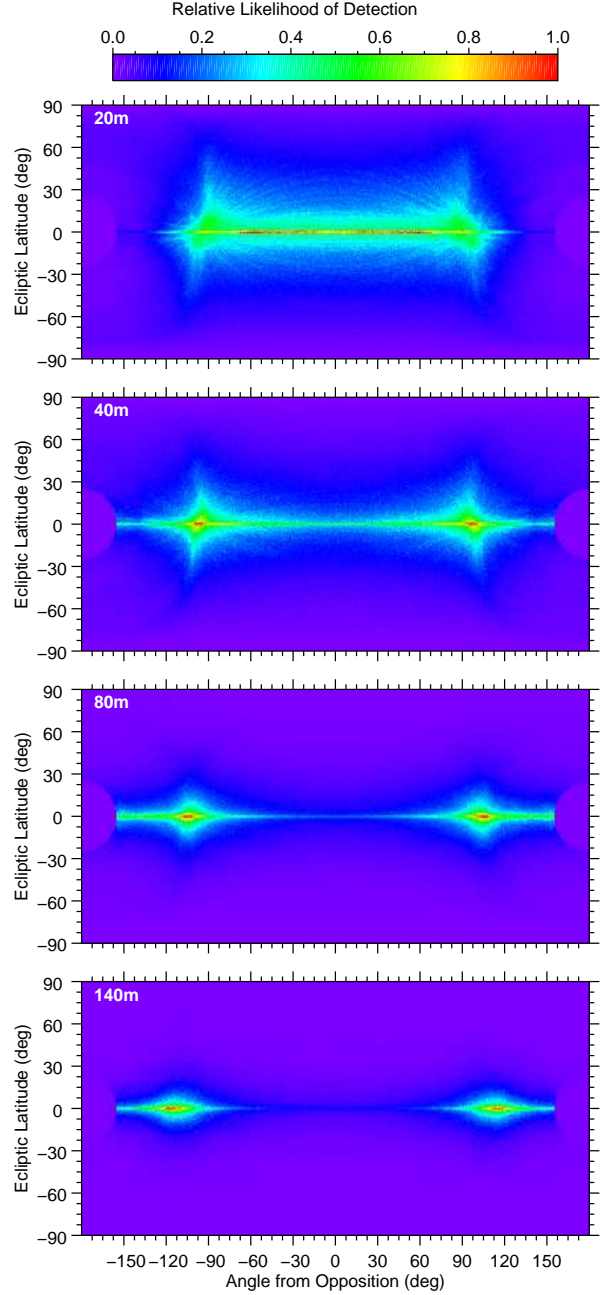


Fig. 5.— Detectability map for virtual impactors with mission option E for different target sizes. Each panel shows where in the sky a target of the given size can be detected. The top panel is for the smallest objects with $D = 20$ m and the bottom panel is for $D = 140$ m. Each map is normalized to 1 at the most likely location. Points with 25° of the Sun are set to zero. At this heliocentric distance, detections are more likely near quadrature with a increasing preference for lower solar elongation angles as the object size increases.

absolute sizes as well as albedo.

Figure 3 shows detection maps for NEAs when surveying from an Earth-like orbit. The overall

pattern is the same in the two cases: small objects are preferred at opposition and larger objects are preferred at lower solar elongations. There is a significant enhancement for larger objects as the solar elongations decreases. Once again, the best region for detection shifts from low to high solar elongation as the object size decreases. The region within 25° is suppressed in all these figures to suppress this extreme low elongation region to make it easier to see the structure in the rest of the sky.

Figures 4 and 5 show the same detection maps but based on the virtual impactor population from Chesley & Spahr (2004) and Vereš *et al.* (2009). As with the NEAs, there is a clear preference for opposition when searching for small objects and quadrature for larger objects. The peak at very low solar elongation is missing in this population and is due to the much more restrictive range of orbits and thus heliocentric position. The virtual impactor population detection zone also differs from the NEA population in being more heavily concentrated along the ecliptic.

These figures suggest that one might significantly enhance the survey detection rate by optimizing the search region. However, these results also show that such optimization will not be equally effective at all sizes. Note that this visualization only summarizes where objects can most readily be seen. The Sentinel survey is designed for self-followup of its discoveries and performance metrics are built on getting a good catalog of orbits. We will return to this important point later in section 10.

7.3. Modified Field of Regard

Several options for modifications to the FOR were investigated. Guided by the zodiacal flux shown in Fig. 1, perhaps the survey could be more effective by always working closer to opposition and thus avoid the higher-background regions closer to 90° from the Sun. Other variations we tried were to avoid the ecliptic poles where the sky density of objects is lower, FOR's that always keep the telescope pointed more nearly perpendicular to the spacecraft-Sun line, and extremely narrow strips near opposition.

Table 9 provides some selected results from the FOR variations examined. The simulations are

run for the baseline mission profile (eg. Venus-like orbit) with only changes to the FOR. The first two columns give the range in solar elongation and the ecliptic latitude range covered. The last two columns indicate the cycle time in days (Δt) and the number of distinct cycles in the 6.5-year survey period (Nt). The rest of the table gives the differential completeness (d) of both $D=140\text{m}$ and $D=30\text{m}$ in percentage units for three different classes of objects. Case #1 shows the performance of the baseline survey. The performance differences clearly depend on the type and size of object considered. When considering either size of NEAs, the peak performance is achieved by the baseline case. The same is true for PHAs and impactors. The results for impactors do show a tie in best performance between the baseline (#1) and a FOR more tightly confined to the ecliptic (#4) at $D=140\text{ m}$ with only a one percentage point increase in completeness at $D=30\text{ m}$. The quadrature cases (13–16) are definitely worse than the baseline and the opposition sliver cases (9–12) are particularly bad.

The information presented in Fig. 2–5 compared to the results in Table 9 brings up a very important point. Sky-plane detection maps are very useful to show where a single-epoch observation is most effective at detecting objects. These have been used very successfully to guide ground-based survey efforts. The detection maps are sufficient to guide the observation planning in the case where the first detection is the sole output of a survey and followup observations are separately handled. When a survey does its own followup the observing constraints are different. For example, if an object had such an orbit that it could only be seen once in the search area, the system would not get a followup observation and the object would not be considered cataloged with a good enough orbit. The survey simulation combines the detection map with the geometric realities of the followup observations needed. As seen in Table 9, the survey performance optimization based on FOR is much weaker than expected from the detection maps alone.

7.4. Exposure Time Modifications

There are two consequences of changing the exposure time: changed time between visits and different sensitivity levels. Longer exposures go

TABLE 9
COMPLETENESS VERSUS FIELD OF REGARD

Case	Sel	Lat	NEA		PHA		Impactors		Δt (days)	Nt
			140	30	140	30	140	30		
1	80–180	± 90	69	4.2	74	6.4	88	19	28	85
2	80–180	± 60	61	2.9	69	4.4	86	15	24	98
3	80–180	± 45	62	2.8	71	4.9	87	16	20	120
4	80–180	± 30	61	2.8	73	6.0	88	18	14	170
5	80–180	± 20	55	2.2	70	5.1	87	17	10	248
6	80–180	± 10	43	1.4	62	3.8	81	13	5	488
7	130–180	± 90	46	2.2	55	4.4	80	15	14	170
8	150–180	± 90	25	0.8	34	1.9	65	09.3	8	283
9	160–180	± 90	16	0.3	25	1.0	55	06.5	6	424
10	170–180	± 90	7	0.1	13	0.5	37	03.5	3	848
11	170–180	± 45	8	0.1	14	0.5	38	03.8	2	1199
12	170–180	± 30	8	0.1	14	0.5	39	04.0	1.4	1695
13	70–140	± 90	65	3.4	71	4.0	85	12	20	122
14	70–140	± 45	62	2.2	70	3.2	85	12	14	172
15	45–120	± 90	58	2.7	65	2.6	78	07.4	21	113
16	45–120	± 45	59	1.9	69	2.6	83	07.5	15	160

NOTE.—The FOR for each case is defined by the range of the solar elongation (Sel) and ecliptic latitude (Lat) covered on the sky. The completion values shown for three sample populations and two sizes (in meters) are given as a percentage of that population. The time required to cover the FOR is given under Δt and Nt is the number of times the FOR is covered during the 6.5 year survey duration.

deeper except when limited by trailing losses. This change will be more effective at quadrature where the target motion is lower than at opposition. After extensive testing with the simulator, the benefit of changing exposure time is minimal. It appears to be most useful as a trade-off against the FOR and the implied cycle interval. The baseline exposure time of 180 seconds when coupled with the choice of telescope and detector characteristics is an excellent choice and we find little reason to modify this aspect of the survey.

8. Simulation Results

This section contains select results from the survey simulations. In the figures and discussion to follow the label ‘V’ is used for the baseline Sentinel mission for its Venus-like orbit, ‘VE’ is used for the same mission profile but with an orbit with perihelion at Venus and aphelion at Earth, ‘E’ is again the Sentinel mission hardware at the Earth’s orbit, and ‘N’ is for an adaptation of the NEOCam mission concept as described in Mainzer *et al.* (2015a) where we use their FOR design and observatory orbit with the rest of the Sentinel mission parameters. In the case of all Sentinel concepts, an object must be observed with a minimum of 28 days orbital arc to be considered a cataloged object and count towards completeness. However, the native cadence of NEOCam is 20 days for a similar criterion. During our modeling of the NEOCam FOR we also used this shorter value. This accommodation gives a slight advantage to the NEOCam FOR scenario with a correspondingly weaker orbit determination for a minimum observational set on an object.

8.1. Baseline Sentinel Mission

Figure 6 provides a summary view of the survey performance of the baseline Sentinel mission. In this graph, and the survey summaries to follow, the cumulative detection performance is shown against target size. The performance here is modeled by physical size and the H magnitude is derived for the purpose of the plot using a standard conversion of $H_V=22.1$, geometric albedo=14%, and $D = 140$ m (Pravec *et al.* 2012). The different colored lines show a wide array of objects with different dynamical groupings. The basic NEA population from Bottke *et al.* (2002) is drawn with a

black line. All other types are varying subsets of the NEA population as described in section 5.5. Some general trends are evident in these results. The Amor population performance is the worst of all at small sizes though it is quite good at larger sizes. This curve shows the transition from a geometry-limited survey at large sizes and a sensitivity limited survey at small sizes. In contrast, the Aten population is systematically better observed at all sizes due to being closer to the observatory and thus easier to observe. The Atira population is even better observed at small sizes but there is a break in the completeness curve around $D > 60$ m where the completeness tops out at 80%. This plateau is a consequence of those objects that happen to remain unobservable for the entire mission due to geometry, that is, Sentinel and those objects are always on the opposite sides of the Sun from each other during the 6.5-year survey. A longer survey would top out at a higher level. Of these populations, the baseline survey is most effect on the ARRM target sample and reaches 100% completeness around $D > 65$ m.

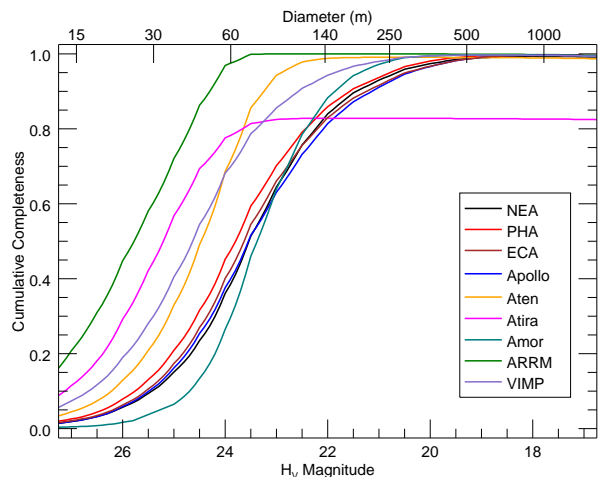


Fig. 6.— Cumulative survey results for the baseline Sentinel mission. The mission duration is 6.5 years and the different curves show different sub-populations of the NEA orbit distribution. H_V is computed from the input diameter using a 14% geometric albedo.

Another instructive view of the survey performance is to look at the cumulative completeness as a function of time. Figure 7 shows such a curve for NEAs (dashed lines) and the Virtual Impactor (VIMP) sample (solid lines). Completeness curves are shown for four different limiting sizes. For the $D > 140$ m impactor population, 90% completeness is reached in about 4 years. If the target sample

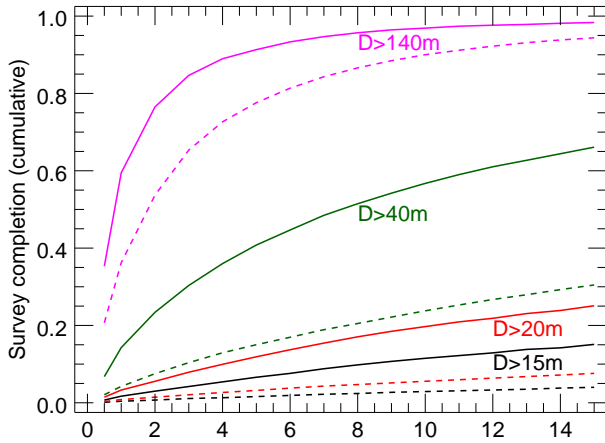


Fig. 7.— Cumulative survey results for the baseline Sentinel mission as a function of survey duration for a variety of limiting sizes. The dashed curves show the results for the full NEA population. The solid curves show the results based on a sample of virtual impactors.

is the entire NEA population it takes nearly 10 years to reach this same completeness level. This plot clearly shows an asymptotic tail for the largest objects that is due to orbital geometry beyond the control of the survey (eg., long orbital periods for some objects). The overall completeness level is clearly seen to decrease when considering smaller sized objects. The cases shown for $D > 15\text{--}20\text{ m}$ objects show these to be in a roughly linear regime where surveying for twice as long will return twice as many discoveries. In this case, two survey instruments with uncorrelated vantage points will detect new objects twice as fast.

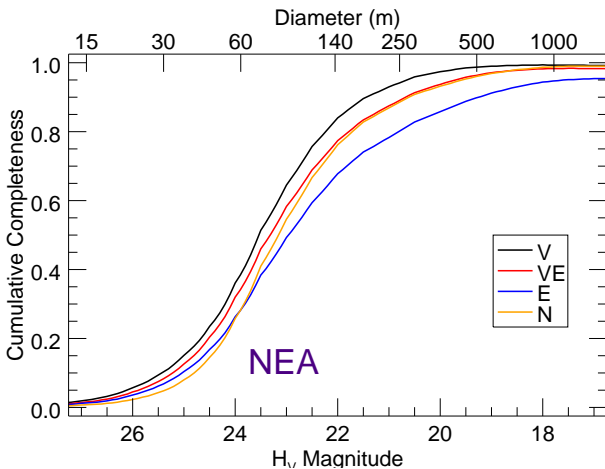


Fig. 8.— Cumulative survey results for NEAs from a 6.5 year survey. H_V is computed from the input diameter using a 14% geometric albedo.

It is instructive to show sub-population results individually for a variety of mission profiles. The

first of these is shown in Fig. 8 for the Bottke *et al.* (2002) NEA population. We use “V” to denote the baseline survey which has a Venus-like orbit. In this case, the baseline mission has the best performance at all sizes for these four mission options but the variation in survey performance is small. The worst concept of this set is for mission option E which reaches a completeness of $\sim 65\%$ for $D > 140\text{ m}$. It is clear that this vantage point requires a significant change in mission design, such as the NEOCam FOR concept, to get better performance. For sizes below 60 m , the NEOCam FOR survey has the lowest performance of these four options. Clearly, if the point of a survey is a measurement of the general population, all of these surveys will constrain the population down to $D = 20\text{ m}$ after careful de-biasing. If planetary defense is a goal where the total number detected is important, there are discriminating choices to be made from these results.

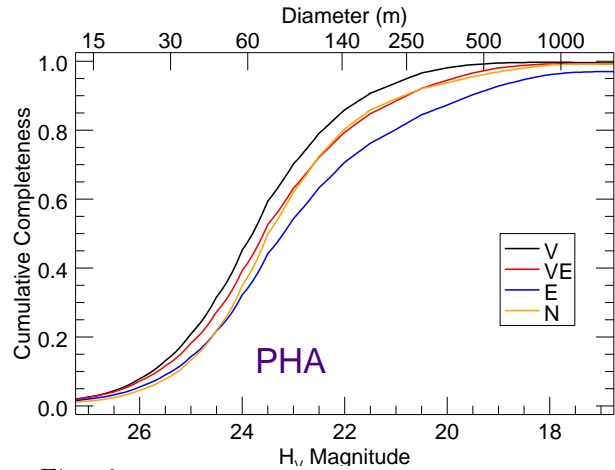


Fig. 9.— Cumulative survey results for PHAs from a 6.5 year survey. H_V is computed from the input diameter using a 14% geometric albedo.

Figure 9 shows the survey performance for potentially hazardous objects defined by an Earth MOID of 0.05 AU or less. As with the NEA population, these curves are all more similar than they are different. Nonetheless, the spread of performance between Sentinel in a Venus-like orbit and option E is slightly larger here for $D = 50\text{ m}$ objects. Once again, there is a drop in the NEOCam FOR performance below 60 m relative to the other options.

The least relevant sub-population for near-term threats to the Earth are the Amors. Again, these curves really are more similar than different but

the consequence of this orbit sample is evident in survey performance (see Fig. 10). The baseline Sentinel has the best performance for $D > 120$ m but has the lowest performance below 50 m. The NEOCam FOR performance is on the lower

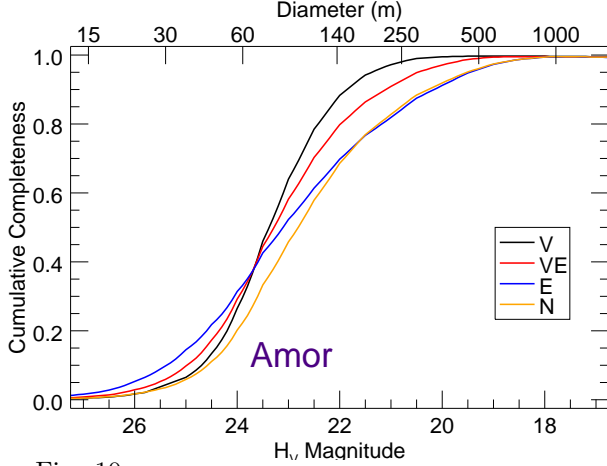


Fig. 10.— Cumulative survey results for Amors from a 6.5 year survey. H_V is computed from the input diameter using a 14% geometric albedo.

boundary of all scenarios and reveals an interesting difference from large object performance where it is identical to option E and small object performance where it is identical to the baseline Sentinel. We conclude that at sizes of $D > 160$ m, the survey performance is insensitive to the FOR or the choice of orbit for the mission. The baseline Sentinel FOR works very well in this case at an Earth vantage point because it looks directly outward where this population is most likely to be found. By being closer, it is more effective on small objects.

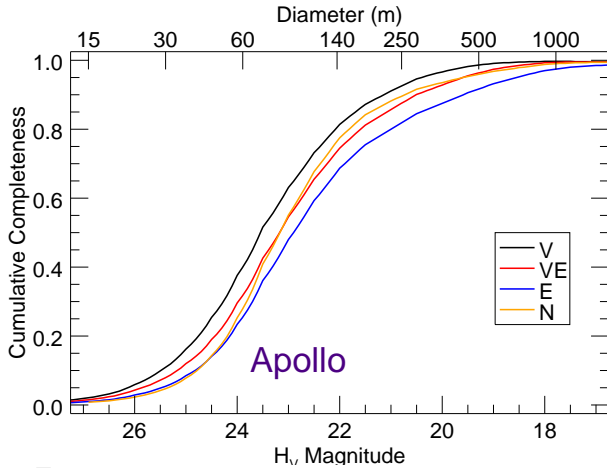


Fig. 11.— Cumulative survey results for Apollos from a 6.5 year survey. H_V is computed from the input diameter using a 14% geometric albedo.

There is very little different about the survey performance for Apollos (see Fig. 11). Once again, Sentinel at Venus and option E bound the range of survey performances with the baseline mission having slightly better performance.

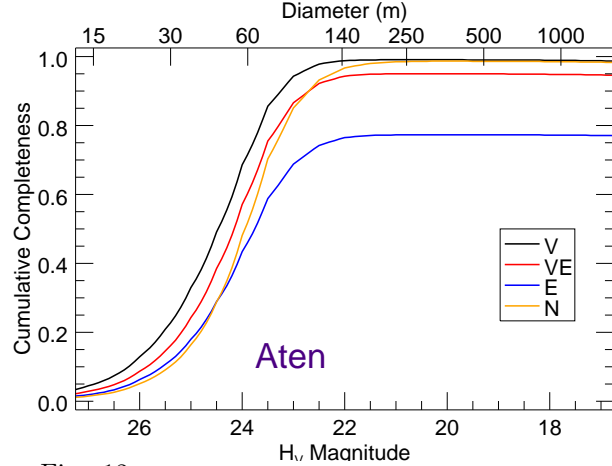


Fig. 12.— Cumulative survey results for Atens from a 6.5 year survey. H_V is computed from the input diameter using a 14% geometric albedo.

Moving inwards, the performance for Atens is shown in Fig. 12. Both the baseline Sentinel FOR and NEOCam FOR surveys work extremely well for $D > 140$ m with essentially 100% completeness. Fundamental geometry limitations seriously affect mission option E. The missed objects just never cross into the FOR. These objects are viewable only at small solar elongations where a FOR like NEOCam provides good coverage. For these large sizes, NEOCam is a very effective option but this advantage drops off to smaller sizes.

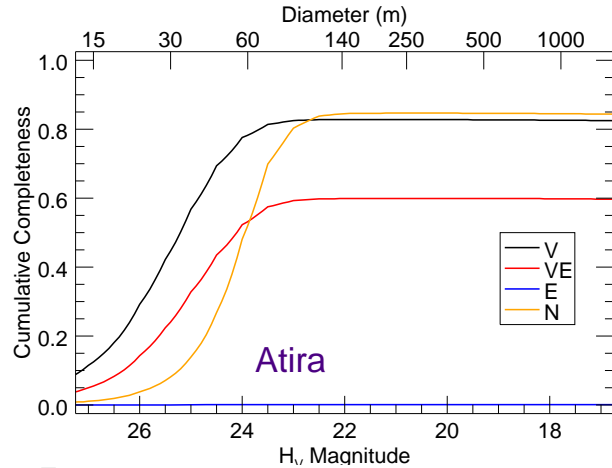


Fig. 13.— Cumulative survey results for Atiras from a 6.5 year survey. H_V is computed from the input diameter using a 14% geometric albedo.

Completing the suite of NEA sub-groups are the Atiras, shown in Fig. 13. These are the objects orbiting closest to the sun and all surveys have geometric limitations for studying these objects. The worst is mission option E which never sees this population at all and the VE option is lower as well because time is spent near the Earth where the Sentinel FOR is less effective. Just as with Apollos, the baseline Sentinel FOR and NEOCam FOR perform well and are effective for large objects and the NEOCam FOR performance drops off more quickly for small objects.

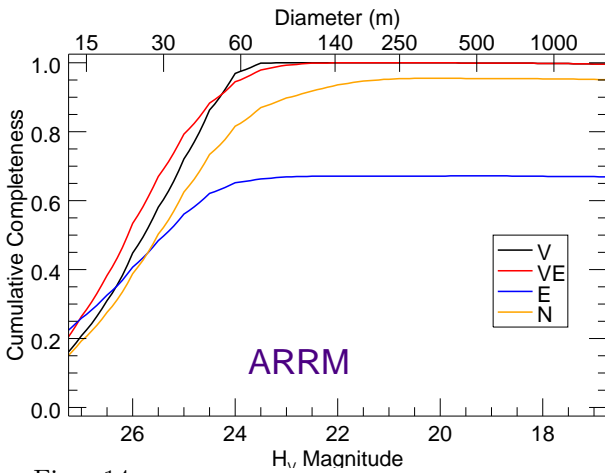


Fig. 14.— Cumulative survey results for ARRM targets from a 6.5 year survey. H_V is computed from the input diameter using a 14% geometric albedo.

A special sub-class of objects, labeled as ARRM targets, is shown in Fig. 14. These objects are special in that they provide low launch energy rendezvous orbits for a spacecraft originating at the Earth. In this case, all options find a significant fraction of these objects. Two of the options, Sentinel-V and Sentinel-VE, all are more than 95% complete for $D > 60$ m and a significant fraction are seen by all mission options down to 15m sizes. We see once again the clear benefit of the NEOCam FOR at an Earth orbiting location compared to option E, which is blind to about 30% of this group.

The final category of virtual impactors is shown in Fig. 15 and is the sample of orbits from Chesley & Spahr (2004) and Vereš *et al.* (2009). Once again we see that all mission options are similarly effective at large sizes. The baseline Sentinel option has the best performance at all sizes and is almost twice as effective as NEOCam at $D > 25$ m.

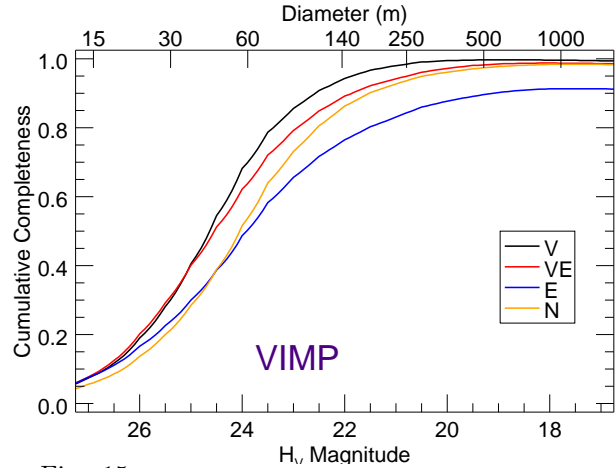


Fig. 15.— Cumulative survey results for Virtual Impactor targets from a 6.5 year survey. H_V is computed from the input diameter using a 14% geometric albedo.

All of the preceding performance plots show completeness alone and are very instructive to see the effectiveness of a given strategy. However, the total number to be detected is equally important. To get a more complete picture we combine the normalization factors from Table 6 with the completeness curves.

From a planetary defense perspective, the most important of these performance curves is the actual impactor population. By combining the results of Fig. 15 and the normalization factor we can show an estimate of the absolute number of objects to be found. Figure 16 shows the result of this calculation. Here we plot the cumulative number of objects that will hit the Earth in the next 100 years as a function of the limiting size. The solid line is the number of objects that are there to be found. Note that this graphic has zoomed in exclusively on the small end of the size distribution. The total number reaches a value of one at $D > 30$ m. For larger size cut-offs the expected number of actual impactors to be found is much less than one. Clearly, the most likely to hit Earth in the next 100 years is in this sub-30 m size range. This is a direct consequence of the overall low impact probability that must be overcome by reaching a point in the size distribution where the number of objects is large enough to compensate. There are very few objects out there to be found that will hit in the next 100 years. These calculations indicate that the total number is ~ 7 for $D > 15$ m. For $D > 20$ m this number has dropped to 3. These calculations imply an im-

pact every 30 years on average for objects down to 20 m in size, roughly consistent with the observed impact rate (Brown *et al.* 2013). Also shown on Fig. 16 are estimates (left axis label) for the number of impactors detected by the baseline Sentinel mission (black dashed curve) and for the VX option (magenta dot-dash curve). The VX option is an improvement of about a factor of two in performance but likely much more expensive than a factor of two due to increased aperture and mission lifetime. With this example in mind it might be more cost-effective to have two Sentinel telescope rather than scale up a single observatory. At the low end of the size range the completeness is low and two observatories will catalog twice as many objects. The scale on the right provides an estimate of how many objects pass within $10 R_{\oplus}$ in 100 years. The choice of $10 R_{\oplus}$ has no special meaning other than such objects still get really close to the Earth and would most likely generate attention without hitting while being a simple number. This example illustrates that there will

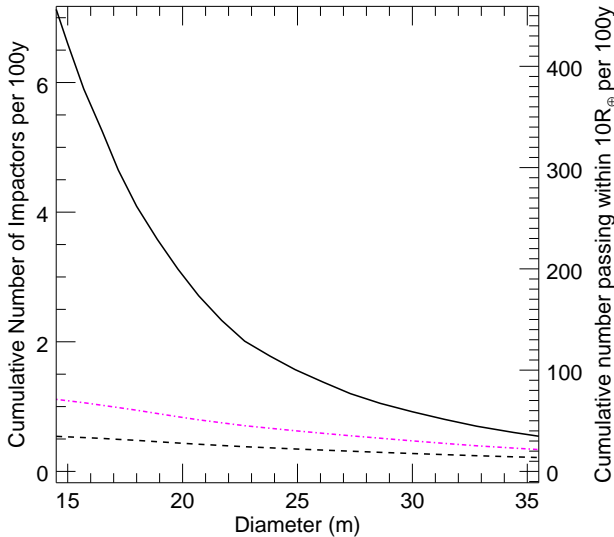


Fig. 16.— Cumulative survey results for Earth impactors from the baseline Sentinel mission. This calculation is for a 6.5 year survey. The solid line is the cumulative number of impactors in 100 years. The black dashed curve is the estimated number of these impactors that would be detected for the baseline Sentinel mission. The magenta dot-dash curve is for the enhanced (VX) Sentinel survey. The scale on the right shows the estimate of how many objects come within $10 R_{\oplus}$ over the same time. H_V is computed from the input diameter using a 14% geometric albedo.

be quite a few objects whose orbits will require close scrutiny to ensure that they are on non-impacting orbits. This estimate counts each object once and does not track multiple passes by

the same object. A summary of key results in this figure is provided in Table 10 along with another common case of objects passing within a lunar distance from Earth. The columns labeled “N” indicate the total cumulative number of objects for that size limit based on the size distribution. The columns labeled N_{det} indicate the number that would be detected by each survey case. This table clearly shows the increasing completeness in the survey with increasing size while also illustrating the rapid decline in the total number that either hit or get close to the Earth over a 100-year period.

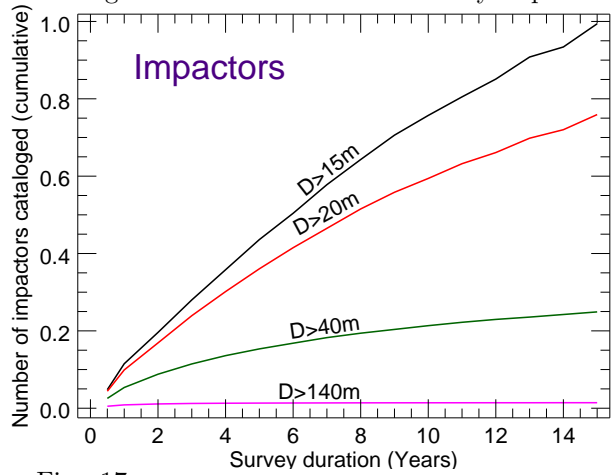


Fig. 17.— Cumulative survey results for Earth impactors from the baseline Sentinel mission as a function of survey duration. Shown here are four curves for different limiting size cutoff for the survey. All results show an estimate of the cumulative number of objects that would be detected during the survey that will be an impactor during the next 100 years. H_V is computed from the input diameter using a 14% geometric albedo.

The expected survey results for impactors is also shown in Fig. 17. In this figure, the number of objects detected is shown as a function of time for four different limiting sizes. The expected number of large impactors is very low, predominantly due to consequences of the size distribution. Sentinel is very good at finding large objects ($D > 140$ m) but there just aren’t that many out there that are impactors. This figure clearly shows the need to effectively search to much smaller sizes to have a significant survey yield of impactors. Within the scope of this study, Sentinel does as good of a job finding these objects as you can do with a single observatory. There are minor performance improvements possible but these come at considerable expense, such as working with a bigger telescope. A more practical way to significantly improve on impactor discoveries is to have more than

TABLE 10
IMPACTORS AND CLOSE FLYBY OBJECTS IN A 100 YEAR TIME INTERVAL

Objects	D>15m		D>30m		D>50m		D>140m		Case
	N	N_{det}	N	N_{det}	N	N_{det}	N	N_{det}	
Impactors	6.6	0.53	0.92	0.28	0.18	0.11	0.014	0.014	Baseline
Impactors	6.6	1.1	0.92	0.47	0.18	0.14	0.014	0.014	VX
within 10 R_{\oplus}	420	34	59	18	12	7.0	0.89	0.89	Baseline
<Lunar distance	15,000	1,200	2,100	640	420	250	32	32	Baseline

NOTE.—This table contains estimates of the absolute numbers of objects in a category and detected in the baseline and VX surveys. The estimates are cumulative numbers above different size cutoffs. The columns labeled “N” is the total number in the category and “ N_{det} ” is the number predicted to be cataloged in a 6.5 year survey.

one survey facility and to have them all in different locations so that their discovery volumes don’t overlap. At the smallest sizes, the completion fraction is low enough that running two surveys will net twice as many impactors. We will discuss this scenario further in the next section.

9. Simultaneous Operation with LSST

Ground-based discovery of NEAs will continue to improve, and the performance of a space survey must be considered in coordination with ground-based results. We have extended our space mission IR model to include ground-based visible observations to permit analysis of the performance improvement made possible by the addition of a space survey. We use the performance of the Large Synoptic Space Telescope (LSST) as a proxy for the performance of all ground-based surveys due to its high potential for discovery of most of the objects that are within reach of ground-based telescopes. We have used this model to evaluate Sentinel’s incremental discovery capabilities for several NEA orbital sub-populations and for various limiting sizes.

9.1. Performance Model for the LSST

The design and anticipated performance for the LSST have been published by the LSST consortium (Ivezić *et al.* 2006). Key parameters that we used to define its performance are summarized in Table 11.

NEA albedo has a strong influence on de-

tectability in the visible wavelengths. Based on observations from WISE (Mainzer *et al.* 2011) we adopted a bimodal distribution, with 50% of the NEOs having a visible geometric albedo of 0.20 and 50% having an albedo of 0.055. This 50:50 ratio holds for NEOs of a given physical size, as used in our modeling, rather than for NEOs of a given absolute magnitude.

We can express the NEO photon flux per unit wavelength interval, F , at the telescope as follows:

$$F = N_{\lambda}(T_{\odot}, \lambda) p_X P(\alpha) \left(\frac{R_{\odot}}{r} \right)^2 \left(\frac{R}{\Delta} \right)^2 \quad (6)$$

where N_{λ} is the emission from the Sun, λ is the wavelength of light, p_X is the bond albedo of the NEO, $P(\alpha)$ is the phase function or brightness as a function of phase angle (α), R_{\odot} is the radius of the Sun, r is the heliocentric distance of the NEO, R is the radius of the NEO, and Δ is the geocentric distance of the NEO. We used the IAU-standard phase function and phase integral as described in Bowell *et al.* (1989) with a typical value of $G = 0.2$ applied to all objects. The blackbody emissivity in photons per unit wavelength is given by

$$N_{\lambda} = \frac{2\pi c}{\lambda^4 [\exp(hc/\lambda kT) - 1]} \quad (7)$$

where T is the effective temperature of the Sun, λ is the wavelength of light, c is the speed of light, h is Planck’s constant, and k is Boltzmann’s constant.

The sky background in the model was designed for spacecraft observations and represents the

TABLE 11
LSST PARAMETERS USED FOR THE SIMULATIONS

Parameter	Value
Detector passband	552-691 nm (<i>r</i> band)
Detector quantum efficiency	0.85
Optical throughput from secondary and mirror losses	0.40
Detector read noise [†]	25 e [−]
Telescope diameter	8.4 m
Minimum SNR for detection	5
Detector fill factor	90%

NOTE.—[†]The estimated read noise is 12 electrons per 15-s exposure. We multiplied by $\sqrt{2}$ to account for two exposures per 30-s integration, and further multiplied by $\sqrt{9/4} = 1.5$ because the oversampling of the LSST focal plane would lead to a 3x3 pixel detection kernel.

scattered light from zodiacal dust seen from Earth orbit. This level is fainter than the sky brightness seen from the ground. We scaled our Earth-orbit value up by a factor of 3 to correspond, on average, to observations with LSST at a zenith angle of $\sim 45^\circ$.

Based on the expected site conditions for LSST (Ivezić *et al.* 2014), we chose a value for the seeing (FWHM of point spread function) of 0.65 arcsec for all LSST observations.

With LSST, the instantaneous FOR is centered on the zenith, with a solid angle determined by the chosen minimum elevation angle. During the course of each night, the instantaneous FOR sweeps up a considerable solid angle. The sky region near opposition is accessible much of the time, with nearly peak sensitivity. As we go farther from opposition, we have a lower duty cycle for access. The zenith angle for those observations will be high and the sensitivity will be reduced. The time-averaged FOR decreases in duty cycle (accessibility) and sensitivity as we go away from opposition, in addition to the sensitivity loss due to sky brightness. In order to use the Sentinel performance model, we approximated this tapered region with a sharp cutoff at $\pm 110^\circ$ in right ascension from opposition and from -90° to $+30^\circ$ in declination.

9.2. Validation of LSST model predictions

With these representations of NEA flux and sky brightness in visible wavelengths, we calculated the performance of the ground-based visible-light LSST telescope for NEA detections. LSST has presented analyses that show it is expected to reach 84% completeness in 10 years on 140-meter PHAs with its nominal observing cadence (Ivezić *et al.* 2007). Completeness levels will be slightly lower for the NEA population, similar to what is seen with the Sentinel analysis. Their measure of completion refers to objects with at least two observations in at least three nights within one lunation. For our Sentinel models we require that the observations extend over more than a Sentinel observing cycle of 30 days in order to provide a sufficiently high quality orbit for future follow-up observations. We apply that same cataloging criterion to the LSST modeling. In our modeling of LSST, a detection consists of 4 *r*-band observations in a lunation and we require detections in two separate lunations for an object to be considered cataloged. The time it takes to cover the LSST FOR four times in a lunation is less than the total time available. This time margin allows for observations with other filters or cadences of lower value for NEA searches. Our model is not sensitive to the exact temporal pattern. These detection and cataloging conditions are different from those used by (Ivezić *et al.* 2007). However,

we feel our choices are reasonable approximations that are easily implemented with our tools.

Our model results for LSST performance is a 73% catalog completeness for NEAs larger than $D=140$ m in 10 years of observations. This is substantially lower than the 82% obtained by the LSST team (www.lsst.org). The difference is primarily due to the differing albedo assumptions. We assumed 50% of NEAs of a given diameter have 5.5% albedo and 50% have 20% albedo as suggested by (Bottke *et al.* 2002). The LSST team used a uniform 14% albedo. When we use the LSST albedo assumption, we predict an 80% catalog completeness.

9.3. Sentinel performance in combination with ground surveys

Both Sentinel and LSST are shown to be highly capable search programs for NEAs. There will be many discoveries common to both the space and ground search programs, and it is important to examine this redundancy in surveys to assess the value of the addition of a space observatory. Redundancy is valuable as both confirmation and extra assurance that objects will not be overlooked but will degrade the combined NEA discovery rate. At the smallest sizes, Sentinels discoveries will be largely uncorrelated with Earth-based detections because, in its heliocentric orbit, Sentinel will observe a different volume of space with unique new NEAs.

In order to compare the incremental advantage of an additional survey, it is necessary to move beyond mere completion statistics to a capability that includes recognizing each discovery as an individual and removing redundant observations of known objects from the second survey. We have performed this analysis for Sentinel using our model of LSST performance and assuming concurrent operation of Sentinel and LSST (2022 start).

Results of our simulations are given in Table 12. The Sentinel mission has a nominal duration of 6.5 years and the LSST project has a nominal survey duration of 10 years. The survey simulations are linked so that we know which objects are common or unique to both surveys. Cumulative completion values are provided for NEAs and virtual impactors for three different limiting sizes. The last three columns give the fraction of the total return

that comes from Sentinel alone (f_S), LSST alone (f_L), and seen by both (f_{S+L}). As seen in this table, the correlation between the samples of the two surveys is highest for $D > 140$ m objects and decreases as the limiting size decreases. At the smallest sizes, Sentinel clearly provides a significant increase in the number of objects cataloged that are not seen by LSST, regardless of what category of object is considered.

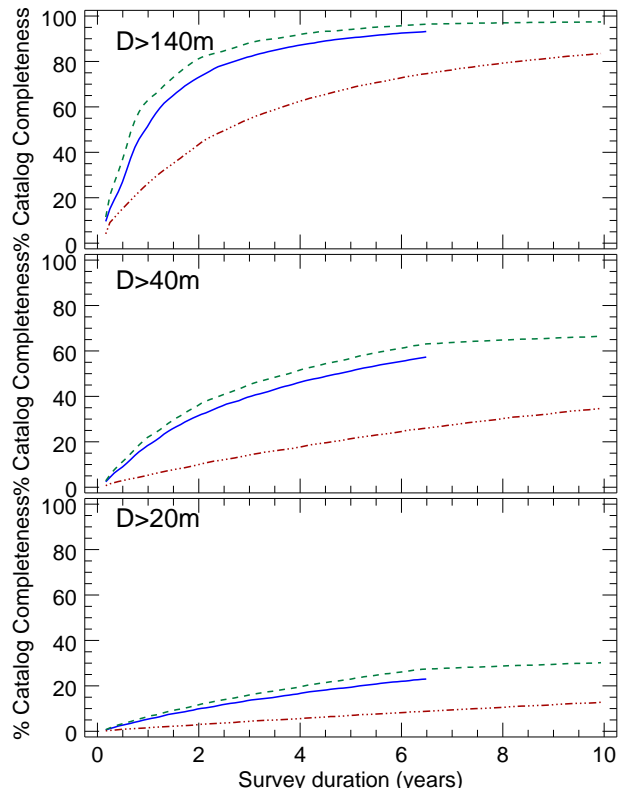


Fig. 18.— Survey completion rates for virtual impactors at different limiting sizes. Shown are completion curves for the baseline Sentinel mission (blue solid lines), LSST (dot-dash red line), and Sentinel and LSST together (green dashed lines). The Sentinel survey only runs for 6.5 years while LSST is shown for 10 years.

Figure 18 provides a graphical summary of the joint performance for these three sizes. Sentinel, designed as a dedicated NEA survey system, has a higher performance level than LSST. Sentinel added to LSST significantly increases the completeness achieved compared to LSST alone. For NEAs larger than 140 meters Sentinel gets 84% completion and LSST also does quite well with 73% completion but the combined performance reaches 93%. As the target size decreases the gap widens somewhat. The redundancy nearly vanishes between these two facilities as the target size

TABLE 12
COMPLETENESS FOR SENTINEL+LSST

Population	S(6.5)	L(10)	S+L	f_S	f_L	f_{S+L}
NEA ($D > 140\text{m}$)	82%	69%	91%	24%	10%	66%
NEA ($D > 40\text{m}$)	27%	15%	34%	56%	21%	23%
NEA ($D > 20\text{m}$)	8%	4%	10%	60%	20%	20%
VIMP ($D > 140\text{m}$)	93%	83%	97%	14%	4%	82%
VIMP ($D > 40\text{m}$)	57%	35%	67%	48%	15%	37%
VIMP ($D > 20\text{m}$)	23%	13%	30%	57%	23%	20%

NOTE.—This table contains the survey performance for Sentinel alone for 6.5 years, S(6.5); LSST alone for 10 years, L(10); and both surveys for their respective durations, S+L. The total number detected in each case is further broken down into the amount seen by Sentinel only (f_S), seen only by LSST (f_L), and seen by both facilities (f_{S+L}).

shrinks. For the impactor population the performance is even better with the combined survey reaching 98% completeness for $D > 140$ m. For the smallest size considered here of $D > 20$ m, the combined survey can reach a completeness of 34% for cataloging impactors and more than half of those are found by Sentinel alone.

We used this model to also assess the redundancy of detections by an IR observatory in the Earth-Sun L1 point with those by ground-based surveys. This case is basically the “N” or NEO-Cam option of Sentinel with a modified FOR that covers 66° to 140° solar elongation. Table 13 shows the result of this calculation for impactors. The combined performance is slightly worse than for the baseline Sentinel case with the combined survey reaching 93% for $D > 140$ m objects. Extending down to 20 m objects, the combined completeness drops to 27% down from 34% for the baseline Sentinel case. The difference is largely due to the redundancy of space discoveries with the discoveries already made by LSST when the space observatory is located near the Earth.

10. Discussion

These tools and results are very useful for establishing survey performance over a range of operating conditions. An important outcome is the ability to provide quantitative performance metrics for different design options. A very strong guiding

principle for the survey is to generate a catalog of objects with high-quality orbits and maximize being able to link other detections with other data. This is a very different strategy from a survey that is optimized to obtain the first detection. Such a narrowly focused first-detection survey requires additional resources to handle the large volume of followup work required for quality orbit determination. A survey that is designed to do its own followup, such as Sentinel, need not be optimized by the same design strategies as a first-detection survey. Indeed, our results indicate that optimizing the field-of-regard to enhance first detection (guided by Figs. 2-5) does not yield a better survey outcome when measured against multi-epoch observations. Such a difference is a consequence of the need for a self-followup survey to find the object at somewhere other than the place where it is most easily seen. Our attempts to optimize the survey based on the FOR show that even the low-density regions near the ecliptic poles have an important contribution to the survey output. The time that might be saved for not observing in those locations only serves to decrease the time between observations that you would already get. The only optimization that is important is in adapting for the preference for opposition or quadrature which is also coupled to the orbit chosen for the observatory.

Considerable effort was given to understanding

TABLE 13
SENTINEL, 1 AU, FOR=66°-140° WITH AND WITHOUT LSST

Population	S'(6.5)	L(10)	S'+L	$f_{S'}$	f_L	$f_{S'+L}$
Imp D>140m	86%	83%	92%	10%	7%	83%
Imp D>40m	45%	35%	54%	35%	17%	48%
Imp D>20m	18%	13%	24%	46%	25%	29%

NOTE.—This table contains survey performance for a modified Sentinel operating at 1 AU looking mostly at quadrature combined with LSST. The cumulative completeness is shown Sentinel alone for 6.5 years, $S'(6.5)$; LSST alone for 10 years, $L(10)$; and both surveys for their respective durations, $S'+L$. The total number detected in each case is further broken down into the amount seen by Sentinel only ($f_{S'}$), seen only by LSST (f_L), and seen by both facilities ($f_{S'+L}$).

our small-object performance and looking for ways to improve the survey in this area. Along the way it was very interesting to see that the large object ($D > 140$ m) performance was nearly as good with all the options we tried. Variations in strategy that included changing cadence, exposure time, telescope aperture, FOR, and FOV, all gave essentially the same answer: good coverage but not quite the 90% coverage desired during the nominal mission duration. The most effective thing for better completeness for large objects is to run the survey for longer. A far more important consideration comes from defining the goals of the survey. The hardest population to get 90% completion on is the NEA group due to their diversity of orbital properties. It is this result that leads to differing goals for this type of survey. For example, here are a few distinct goals: 1) deduce the population of asteroids in the near-Earth region of the solar system, 2) find all of the asteroids in the near-Earth region, or 3) find all of the objects that pose an imminent threat to the Earth. This is by no means an exhaustive set of possible goals but serves to frame the discussion.

Case #1, elucidating the population, is perhaps the easiest task of the three since a survey only needs to find enough objects such that the error introduced during the de-biasing of the survey data are small enough for the subsequent scientific investigation. Arguably, we already have enough objects cataloged to permit successful de-biasing of the survey to directly constraint our knowledge of the population in its overall properties. Un-

certainities of a factor of a few may still be possible down to $D > 20$ m and there are still questions about the actual shape of the distribution but the Earth impact record gives us very important ground-truth for the modern era. Also, this case has no particular urgency for its completion. Given enough time, efforts from relatively inexpensive ground-based efforts will eventually solve this particular problem. Indeed, most of what we know now comes from ground-based efforts.

Case #2, finding NEAs down to a limiting size, is a difficult task that is limited nearly as much by orbital properties as the detection strategy. The full NEAs orbit distribution includes objects with either long periods or other complicating geometric constraints that leave them impossible to detect almost all of the time without extreme effort. In this case, reaching a 90% completeness level will require survey durations matched to the orbital outliers. Furthermore, the vast majority of these objects bear no threat against the Earth. Again, if the goal is a scientific investigation of the population, completeness is not required. Completeness is a compelling issue when weighed against the threat of impact on the Earth. This argument brings us to case #3.

If the goal of NEA surveys is to identify actual threats to the Earth, such surveys should be optimized for this outcome. Clearly, with such a focus, an object that won't hit the Earth in the next billion years should be of no concern when designing the survey. However, the George E. Brown act

survey mandate does just that by “requiring” detection of NEAs for the mandate to be fulfilled, all in the name of identifying threats to the Earth.

A survey dedicated to threatening objects takes on a very different form from a more general NEA survey. The NEA population can be split up into three distinct groups. The first group contains those objects that *will* hit the Earth in the next 100 years – call these objects the set of impactors. The second group contains objects that will become an impactor 100 years or more in the future up to some limiting timescale of interest – call these the set of future impactors. The third group is comprised of those objects posing no threat at all – call these the background population. The choice of 100 years for the time horizon of concern is chosen to loosely match the timescale for chaotic evolution of the NEA orbits. Within a 100 year period from now we can, with sufficient data, accurately predict an object’s motion and know with certainty that it either will or will not impact the Earth. Beyond 100 years the chaotic nature of the orbits precludes firm knowledge, only a likelihood of impact. This 100 year window is perhaps not rigorously correct but serves as a commonly used guideline for the prediction threshold. For the purposes of this discussion we consider the 100 year limit to be a hard cutoff even though the real limit depends on the actual object and its size, not to mention the quality of its orbit estimate.

The set of impactors is very small and is a reasonably well known number just from recent history. As shown in Fig. 16, current estimates indicate there are 7 objects down to 15 m that will impact the Earth in the 100 years following the survey. The set of future impactors would thus be 700 if the time-horizon of concern were set to be 100 centuries. That is still a small number. Of course, this set cannot be deterministically known. The chaotic evolution of the impactor orbits will dictate a mean probability of impact for this group and those that will be close to, but not actual impactors. If, for example, the mean probability were as low as 10% in this group, then the sample of objects worth tracking would then be 7000 objects. In reality, this probability will evolve from being deterministic at 100 years out to being ever less certain as you look further into the future. These two sets of objects are in stark contrast by numbers against the third category

of background NEAs. According to recent estimates by Boslough *et al.* (2015), there are nearly 100 million objects with $D > 15$ m. The overwhelmingly vast majority of objects out there to be found are those that will not ever strike the Earth. Our analysis shows there are ways to bias a survey toward improved efficiency of finding impactors at the expense of not finding as many other non-threatening types.

One result that has become very clear during this analysis is just how big the problem is for finding impactors. There are many steps along the way toward planetary defense. The first step is a wide-field survey. Ideally, surveys should continue until all the objects are found but subsequent steps can begin before the survey process is completed. The output of the survey process is a catalog of objects with orbits of varying quality. These orbits will range from very well determined to very poorly determined. For any objects with a non-zero impact probability, we need to continue with long-term followup observations. Additional observations will reduce the list of candidate impactors. This followup work is distinguished from the initial survey by the need to re-observe an already known object. Some objects will be well enough known to permit a targeted observation while others will effectively require rediscovery. In the end, the requirement is to get a minimum astrometric arc that will prune the candidate list down from 10^8 to something manageable for concerted high-precision work. The details of how long the observational arc must be are beyond the scope of this work but should be addressed, especially in light of what the astrometric data quality will be like once the Gaia star catalog becomes available. It may well be that completing this initial cataloging step may require two separate all-sky surveys separated by some period of time, say 10 years, to ensure long-arc orbital constraints on everything.

The final step comes when one of the candidate list is then found likely to be on a collision course with Earth. From there the mitigation work begins with a definite goal. Given the nature of the size distribution of NEAs, very small objects will likely be the first identified. The discovery of a small Chelyabinsk-sized object would actually be the ideal for our first attempt at space-based mitigation since the impact effects can be protected

against by relatively simple civil defense actions local to the affected area. The inescapable conclusion here is that planetary defense is a long-term task and really has no end. The startup phase of getting complete catalogs is the hardest part and will require many decades of effort, or longer. The Sentinel mission we have studied here is a big step along the way. By combining its efforts with a complementary LSST effort we can improve the cataloging rate and reach a sample size that is likely to net the first actual impactor.

11. Conclusions

We have looked at many variations for Sentinel and find that, for small impactors, the nominal orbit provides a very effective location for surveying and we do not find any options for substantial improvement that do not markedly increase the mission cost – aperture of the telescope being the most important. In particular, Sentinel can reach 50% completeness for impactors larger than 40 meters. Observatory location is not critical for any sub-population except for impactors and ARRM targets. In particular, observing from an Earth-neighborhood location is inferior to the interior orbit for objects of interest to planetary defense or human exploration targets. One clear lesson from this work is the need to be concerned with modeling performance down to a $D = 15 - 20$ m size range for these two goals. For planetary defense, this conclusion is supported by the fact that most near-term threats come from the smallest objects and you have to get down to this small size before an event is likely in the next 100 years.

Depending on the current completeness level of any population, optimization of a survey could lead to changes in the survey design if only the undiscovered population were considered. If a survey were merely an incremental improvement, this could be a very important consideration. Our survey modeling leads to guidance on an optimized strategy assuming you haven’t yet found any objects. The real situation is somewhere in the middle between these two cases for Sentinel but closer to the “new” survey end of the spectrum due to working to much smaller sizes and working in the infrared where the biases against finding low albedo objects are removed. Modeling the undiscovered sub-populations will be left

to future work, if warranted.

Working to such small sizes leads to a fundamentally higher discovery rate than is currently taking place. The reality of higher discovery rates requires significant effort for followup as well and new surveys really must work to do their own followup as much as possible. In our survey design we also make a strong distinction between detection and cataloging. When modeling survey performance it is also important to track the observational arc that would be obtained on any newly discovered object. There is a minimum arc required to ensure linking against other later observations and this point is often overlooked. For our survey performance metrics we insist on a minimum arc of 28 days but this value is more of a guideline than a hard requirement. The minimum required arc needed to claim an object is cataloged might be worth additional study.

Object detection is indeed easier in some locations in the sky, – the so-called “sweet spots” where the probability of detection is at its peak (cf., Chesley & Spahr 2004; Vereš *et al.* 2009). As shown in Figures 2–5, the discovery sweet spot depends on the observatory location and it also depends on object size and aperture. It is clear from our analysis that the best detections of an object will most likely come from these areas of the sky but the minimum arc length goal pushes the followup observations into other regions of the sky. For this reason, the FOR of a survey that does its own followup must necessarily cover more sky than just the sweet spots.

NEA surveying is a difficult enough task, particularly at the small size range, that cost effective survey plans need to consider combining efforts from other facilities. This combined survey strategy can be accomplished in many ways. One easy example is to fly more than one space observatory and placed in different locations in space. For instance, a set of three Sentinel telescopes in a Venus-like orbit spaced by 120° of longitude would be three times as fast at finding the objects down to $D = 15$ m. This group would also be much more effective at followup and give much longer observational arcs for the resulting object orbit catalog. Such strategies are very powerful but also quite expensive. In the near term, any such space-based facility really should work to be complementary to ground-based surveys, represented in our study

by LSST so that both surveys can add the largest number of objects to our NEA catalogs. In the case of Sentinel plus LSST, we find the combined survey will find more than 70% of asteroid impactors larger than 40 meters. The choice of orbit for a survey telescope also an important consideration.

Our modeling of the combined Sentinel plus LSST performance will be a catalog of perhaps 1000's of possible impactors that will require continued, potentially long-term followup observations to sift out the real impactors from close misses. Additionally, this catalog will permit routine prediction of future close passes for continued study, significantly reducing the number of objects that will sneak up on the Earth without warning before its first detection.

We are poised on the threshold of a huge step forward in NEA surveys, a step that will begin to reveal a more complete picture of the objects in space around us. This step will come from a space-based approach combined with ground-based observations, especially LSST. The task of mitigating against impacts does not end with this step. Continued surveys will be required for a while to get good observational arcs on all discovered objects as well as continuing to strive for ever better completeness for small objects. This initial phase of catalog will likely require at least two such survey efforts separated in time. After that work, followup becomes ever more increasingly targeted and no longer requires all-sky surveys. Nonetheless, protecting the Earth against impactors is a long-term and unending task and doing so is clearly within our grasp.

Funding for this work provided by the B612 Foundation and its Founding Circle donors (K. Algeri-Wong, B. Anders, G. Baehr, W. K. Bowes Jr. Foundation, B. Burton, A. Carlson, D. Carlson, S. Cerf, V. Cerf, Y. Chapman, A. Denton, E. Dyson, A. Eustace, S. Galitsky, E. Gillum, L. Girand, Glaser Progress Foundation, D. Glasgow, J. Grimm, S. Grimm, G. Gruener, V. K. Hsu & Sons Foundation Ltd., J. D. Jameson, J. Jameson, M. Jonsson Family Foundation, S. Jurvetson, D. Kaiser, S. Krausz, J. Leszczenski, D. Liddle, S. Mak, G. McAdoo, S. McGregor, J. Mercer, M. Mullenweg, D. Murphy, P. Norvig, S. Pishavar, R. Quindlen, N. Ramsey, P. Rawls Family Fund, R. Rothrock, E. Sahakian, R. Schweickart, A. Slater, T. Trueman, F.B. Vaughn, R.C. Vaughn, B. Wheeler, Y. Wong,

M. Wyndowe plus 8 anonymous donors). Thanks to Lowell Observatory and E. L. G. Bowell and L. H. Wasserman for the use of the `astorb.dat` database, funded by NASA grant NAGW-1470 and the Lowell Observatory endowment.

REFERENCES

- Bottke, W.F., Morbidelli, A., Jedicke, R., Petit, J.-M., Levison, H., Michel, P., and Metcalfe, T.S. 2002. *Icarus* 156, 399.
- Boslough, M., Brown, P., and Harris, A. 2015. IEEE Aerospace Conference, Big Sky, MT. doi 10.1109/AERO.2015.7119288
- Bowell, E., Hapke, B., Domingue, D., Lumme, K., Peltoniemi, J. and Harris, A. W. 1989. *Asteroids II*, eds. R.P. Binzel, T. Gehrels, M.S. Matthews, Univ. of Arizona Press, pp 524-556.
- Brown, P.G., Assink, J.D., Astiz, L., et al. 2013. *Nature* 503, 238.
- Cellino, A., Muinonen, K., & Tedesco, E. F. 2004, *Advances in Space Research*, 33, 1576.
- Chesley, S.R., Spahr, T.B., 2004. Earth-impactors: Orbital characteristics and warning times. In: Belton, M.J.S., Morgan, T.H., Samarashinha, N.H., Yeomans, D.K. (Eds.), *Mitigation of Hazardous Comets and Asteroids*. Cambridge University Press, Cambridge, pp. 22-37.
- Granvik, M., Virtanen, J., Muinonen, K. 2009. *M&PS* 44, 1853.
- Ivezić, Z., J. A. Tyson, M. Jurić, J. Kubica, A. Connolly, F. Pierfederici, A. W. Harris, E. Bowell, and the LSST Collaboration. 2007. LSST: Comprehensive NEO Detection, Characterization, and Orbits. In *Near Earth Objects, Our Celestial Neighbors: Opportunity and Risk Proceedings International Astronomical Union Proceedings*, edited by A. Milani, G. B. Valsecchi and D. Vokrouhlický.
- Ivezić, Z., Tyson, J. A., Jurić et al. 2006. IAU Symposium 236 "Near Earth Objects, Our Celestial Neighbors: Opportunity and Risk", *Proc IAU Symp No. 236*, p. 353.
- Ivezić, Z., Tyson, J. A., Abel, B. et al. 2014. <http://arxiv.org/pdf/0805.2366.pdf>
- Jedicke, R. 1996 *AJ* 111, 970.

- Jedicke, R., Morbidelli, A., Petit, J., 2003. *Icarus* 161, 1733.
- Jedicke, R., Magnier, E.A., Kaiser, N., Chambers, K.C., 2006. Proceedings IAU Symposium No. 236. Cambridge University Press, Cambridge, Milani, A., Valsecchi, G.B., Vokrouhlický, D. (Eds.), pp.341352.
- Jedicke, R., Granvik, M., Micheli, M., Ryan, E., Spahr, T., and Yeomans, D. K., 2015. In *Asteroid IV* (P. Michel *et al.*, eds.) pp. 795-813.
- Kelsall, T., Weiland, J. L., Franz, B. A., Reach, W. T., Arendt, R. G., Dwek, E., Freudenreich, H. T., Hauser, M. G., Moseley, S. H., Odegard, N. P., Silverberg, R. F., and Wright, E. L. 1998. *Apj* 508, 44.
- Koch, D.G., Borucki, W.J., Basri, G., Batalha, N.M., Brown, T.M., Caldwell, D., Christensen-Dalsgaard, J., Cochran, W.D., DeVore, E., Dunham, E.W., Gautier, T.N., III, Geary, J.C., Gilliland, R.L., Gould, A., Jenkins, J., Kondo, Y., Latham, D.W., Lissauer, J.J., Marcy, G., Monet, D., Sasselov, D., Boss, A., Brownlee, D., Caldwell, J., Dupree, A.K., Howell, S.B., Kjeldsen, H., Meibom, S., Morrison, D., Owen, T., Reitsema, H., Tarter, J., Bryson, S.T., Dotson, J.L., Gazis, P., Haas, M.R., Kolodziejczak, J., Rowe, J.F., Van Cleve, J.E., Allen, C., Chandrasekaran, H., Clarke, B.D., Li, J., Quintana, E.V., Tenenbaum, P., Twicken, J.D., Wu, H. (2010). *ApJL* 713, L79.
- Larson, S. 2007, in IAU Symp. 236, Near Earth Objects, our Celestial Neighbors: Opportunity and Risk, ed. G. B. Valsecchi, & D. Vokrouhlický, (Cambridge: Cambridge University Press), 323.
- Lu, E.T., Reitsema, H.J. Troeltzsch, J. Hubbard, S. 2013. *New Space* 1, 425.
- Mainzer, A., Grav, T., Bauer, J. *et al.* 2015a. *AJ* 149, 172.
- Mainzer, A., Bauer, J., Grav, T., *et al.* 2015b. Space-Based Infrared Discovery and Characterization of Minor Planets with NEOWISE. In Handbook of Cosmic Hazards and Planetary Defense, Edited by J. Pelton and F. Allahdadi, Springer Intl. Pub, Switzerland, p. 583-611.
- Mainzer, A., Grav, T., Bauer, J. *et al.* 2011. *ApJ* 743 156.
- NRC Committee to Review Near-Earth Object Surveys and Hazard Mitigation Strategies; National Research Council, 2010. Defending planet Earth: near-Earth object surveys and hazard mitigation strategies, 152 pp. ISBN 978-0-309-14968-6
- Pravdo, S.H., Rabinowitz, D.L., Helin, El.F., and 11 co-authors, 1999. *AJ* 117, 1616.
- Pravec, P., Harris, A.W., Kušnirák, P., Galád, A., and Hornoch, K. 2012. *Icarus* 221, 365.
- Reitsema, H.J. and Lu, E.T. 2015. Sentinel: A Space Telescope Program to Create a 100-Year Asteroid Impact Warning. In Handbook of Cosmic Hazards and Planetary Defense, Edited by J. Pelton and F. Allahdadi, Springer Intl. Pub, Switzerland, pp. 570-581.
- Spencer, J.R., Lebofsky, L.A., & Skyes, M.V. 1989. *Icarus* 78, 337.
- Spencer, J.R. 1990. *Icarus* 83, 27.
- Stokes, G.H., Evans, J.B., Viggh, H.E.M., Shelly, F.C., Pearce, E.C., 2000. *Icarus* 148, 21.
- Tedesco, E.F., Muinonen K., and Price S.D. (2000). *Planet. Space Sci.* 48, 801.
- Vereš, P., Jedicke, R., Wainscoat, R., *et al.* 2009, *Icarus*, 203, 472.
- Willson R.C., C.H. Duncan, and J. Geist 1980, *Science* 207, 177.